Combustion Science and Technology, Available online 18 April 2025
DOI:10.1080/00102202.2025.2492743

Investigation of ash and combustion characteristics during co-combustion of coal and solid recovered fuel in a laboratory-scale combustor

Adi Prismantoko[a*], Feri Karuana[a], Moch Zulfikar Eka Prayoga[b], Arif Darmawan[b], Muhammad Akhsin Muflikhun[c], Nimas Mayang Sabrina Sunyoto[d], Mingming Zhu[e], Muhammad Aziz[f], Hariana Hariana[b**]

[a] Research Center for Process and Manufacturing Industry Technology, National Research and Innovation Agency, South Tangerang 15314, Indonesia

[b] Research Center for Energy Conversion and Conservation, National Research and Innovation Agency, South Tangerang 15314, Indonesia

[c] Department of Mechanical and Industrial Engineering, Gadjah Mada University, Yogyakarta 55281, Indonesia

[d] Faculty of Agricultural Technology, Brawijaya University, Malang 65145, Indonesia

[e] School of Water, Energy and Environment, Cranfield University, Cranfield, Bedfordshire, MK43 0AL, UK

[f] Institute of Industrial Science, The University of Tokyo, 4-6-1 Komaba, Meguro-ku, Tokyo 153-8505, Japan

*Corresponding author: adi.prismantoko@brin.go.id (A. Prismantoko)

**Corresponding author: hariana@brin.go.id (H. Hariana);

Abstract

Population growth and limited landfill area increase the problems associated with municipal solid waste (MSW). The MSW conversion into solid recovered fuel (SRF) improves the calorific value which has the potential to be used as a power plant boiler fuel. This study investigated ash deposition and combustion characteristics during co-combustion of coal and SRF at various dosages (5, 10, 15, 20, and 25 wt%). Thermogravimetry analysis, preliminary risk assessment, and morphology analysis of ash deposits are comprehensively performed. The study revealed that based on combustion performance, SRF blends up to 20 wt% show slightly altered burnout temperatures compared to coal combustion, whereas, at 25 wt%, the combustion temperature increases significantly. On the initial risk assessment,

Published by Taylor & Francis. This is the Author Accepted Manuscript issued with: Creative Commons Attribution License (CC:BY 4.0).
The final published version (version of record) is available online at DOI:10.1080/00102202.2025.2492743. Please refer to any applicable publisher terms of use.

the samples tested had a low to medium risk of slagging. Morphological observations show that fine, irregular, and unmelted particles dominated coal ash deposits, while SRF ash deposits were dominated by melted and agglomerated particles. The melted particles gradually increase as the dosage of SRF in the mixture increases. Low melting temperature element-rich particles start to be observed at doses higher than 10 wt%. At 25 wt% SRF blends, material degradation was observed with the presence of Cr in the ash deposit. Overall, co-combustion over 10 wt% SRF shows results that should be considered, particularly the increase in sintering ash that can cause problems in the boiler pipes. This study provides insight into the optimum dosage suitable for blending SRF and coal in power plant boilers.

Keywords*: ash morphology, element composition, material degradation, sintering ash, thermochemical analysis*

1. Introduction

Problems related to municipal solid waste (MSW) increase as the population grows and landfill space becomes scarce. Research conducted by Qonitan et al. (2021) revealed that, based on data in Indonesia in 2018, more than 1,700 tonnes per day of MSW average per city was produced. In another study by Vekemans and Chaouki (2016), worldwide MSW production in 2025 will reach more than 2 billion tonnes annually. As a solution to these problems, several technologies such as combustion, gasification, pyrolysis, and hydrothermal can be applied (Babu et al. 2021). One of the simple and effective technologies is combustion technology. MSW can be combusted directly or sorted to convert to fuel and then processed into solid recovered fuel (SRF) (Sugiyono et al. 2022). MSW has a calorific value of about 19 MJ/kg (Nasrullah et al. 2015; Vekemans and Chaouki 2016; Zhang et al. 2018), while SRF has a calorific value of 12–25 MJ/kg (del Zotto et al. 2015; Prismantoko et al. 2024a; Wu et al. 2011). Other MSW derivatives, such as refuse-derived fuel (RDF), have a calorific value of 11–20 MJ/kg (Karpan et al. 2021; Maj et al. 2022; Prismantoko et al. 2024b). The high calorific value of SRF and other MSW-derived waste that approaches the calorific value of low-rank coal makes SRF promising as an alternative or blended fuel in coal-fired power plants (CFPP). In addition, with the high content of biodegradable materials such as paper, wood, and textile generally having lower sulfur and

nitrogen content than coal, the combustion of SRF can reduce flue gas emissions in CFPP (Vekemans and Chaouki 2016; Wu et al. 2011). However, applying SRF as an alternative fuel in CFPP is also challenging. Due to its different characteristics from coal, the CFPP boiler is designed to be fuelled by coal. The high chlorine and alkali content in SRF can lead to corrosion and ash deposition, resulting in boiler pipe problems during combustion (Kaniowski et al. 2022; Viklund et al. 2013).

To ensure the boiler operation does not experience problems due to using SRF as fuel, it is necessary to conduct a comprehensive study before being applied to the actual scale boiler. Studies on SRF combustion, both single and co-combustion, have been performed extensively. Combustion characterization was carried out by Sever Akdağ et al. (2016), finding that the main decomposition during refuse-derived waste combustion occurs between 200 and 600 °C. In addition, combustion is completed at around 700 °C with 20% char remaining at the end of the process. A study by Conesa and Rey (2015) showed that hemicellulose decomposes during MSW combustion at temperatures between 200–250 °C, while cellulose decomposes at 400 °C. Wu et al. (2020) have stated that the pyrolysis performance of SRF will increase as the heating rate increases. Viczek et al. (2021)discovered that most of the CO_2 released during SRF combustion comes from the combustion process, but further release results from endothermic reaction due to carbonate decomposition in the sample starting at 600 °C. Regarding the ash observation, research conducted by Wojtaszek et al. (2021) revealed that co-combustion of 10 wt% coal-SRF showed the addition of unfused, porous, and sooty particles. Ściubidło et al. (2019) found that coal and SRF co-combustion ash deposits are dominated by coarse, angular, irregular, drossy, and flaky particles. Meanwhile, in another study, Tang et al. (2016) found that municipal solid waste combustion is dominated by fine and spherical particles rich in Al, Si, K, and Na. Moreover, our previous study showed that Ca-rich and agglomerated particles increased by adding 15 wt% SRF into different coals (Prismantoko et al. 2024a). The addition of 15 wt% SRF to the coal increases the elements that contribute to the lowering of the ash fusion temperature. In another separate study, Prismantoko et al. (Prismantoko et al. 2024b) observed the separation of biodegradable and non-biodegradable rich waste, where melted particles and aggregates were absent in the coal blend with 5

wt% biodegradable rich waste but still observed in the blend with 5 wt% in non-biodegradable rich waste. More detailed studies on the co-combustion of coal and solid waste can be seen in Table 1.

Although other studies have examined the single and co-combustion of coal and SRF, critical knowledge gaps persist regarding the challenges associated with coal-SRF co-combustion, particularly given the diversity of coal types and the heterogeneous composition of SRF. Previous research has also discussed material degradation caused by ash from the combustion of coal blends with SRF up to 25 wt% (Karuana et al. 2024a). However, these studies primarily focused on the degradation of the material's protective layer, neglecting a comprehensive analysis of combustion characteristics and the mechanisms driving ash deposit formation. Notably, at a mixture of 15 wt% SRF in coal, the material experienced significant degradation. Therefore, this study focuses on combustion performance, analyzing the morphology and elements of ash deposits to determine the effect of coal and SRF blends at various ratios on slagging, fouling, and corrosion tendencies. Combustion performance was analyzed using a thermogravimetric apparatus, while ash morphology analysis was performed using scanning electron microscopy and energy-dispersive X-ray spectroscopy (SEM-EDS) instrumentation. This study is expected to provide a valuable reference for addressing waste management challenges, especially regarding combustion characteristics and ash deposition during the co-combustion of coal and SRF at various ratios.

Table 1. Research benchmarks on coal and SRF/RDF/MSW co-combustion

References	Fuels	Testing tools	Dosage of waste	Findings
(Zhang et al. 2018)	Coal and MSW	DTF (1300 °C)	7.5, 15, 20, and 25 wt%	Increasing the MSW dosage resulted in a rougher fly ash surface due to condensation and accumulation of fine particles. In addition, a decrease in ash fusion temperature is observed, and an increase in Fe, Cl, and S content in the fly ash.
(Ściubidło and Nowak 2018)	Coal and SRF	CFB (800–900 °C)	1, 5, 10, and 20 wt%	Ash particles during co-combustion are dominated by irregular, coarse, flaky and drossy particles. On the other

References	Fuels	Testing tools	Dosage of waste	Findings
				hand, subangular particles and irregularly shaped unburned carbon particles are found in fly ash. Quartz, anhydrite and illite are found in all test samples, while mullite are unobserved.
(Wasielewski et al. 2020)	Coal and SRF	Stoker boiler (700–900 °C)	10 wt%	Porous particles, unburnt inert minerals, and cenospheres minerals are observed in coal fly ash, while fine crystalline porous and amorphous particles dominated the SRF blended fly ash. Unburned carbon increased during SRF co-combustion.
(Mlonka-Mędrala et al. 2021)	Coal and RDF	CFB (800–900 °C)	40 wt%	Irregular quartz-rich particles with some melting and agglomeration particles are observed during co- combustion. EDS analysis showed the main components are Si, Al, Ca, Fe, Na, and S.
(Wojtaszek et al. 2021)	Coal and SRF	Stoker boiler (800–1100 °C)	10 wt%	Unburn carbon increases with the addition of SRF to coal. Coal fly ash is dominated by fused, dense, and anisotropic particulate, after the addition of 10 wt% SRF, unfused, porous, and isotropic particles increase.
(Isaac and Bada 2022)	Coal and RDF	HTF (850 °C)	15, 30, 50, and 75 wt%	Shredded sponge and chip particles are observed in RDF ash, while Coal is dominated by fine and coarse particles. During co-combustion, the ash is dominated by cluster particles and agglomerates with low melting point. The slagging and fouling indices show that as the percentage of RDF in the blend increases, the tendency of slagging and fouling increases.
(Hariana et al. 2023)	Coal, SRF, and another biomass	DTF (1200 °C)	25 wt%	Co-combustion of coal and SRF at 25 wt% showed a high risk of slagging with the presence of molten and aggregated particles

References	Fuels	Testing tools	Dosage of waste	Findings
				with low melting temperatures compared to other biomasses. In addition, it has a higher corrosion propensity.
(Shin et al. 2023)	Coal and Bio-SRF	CFB (800 °C)	10, 20, and 30 wt%	As the waste mixture ratio increased, the calorific value and unburned carbon decreased, the ash content increased. In addition, there is no change in boiler and combustion efficiency.
(Prismantoko et al. 2024a)	Coal and SRF	DTF (1200 °C)	15 wt%	The addition of 15 wt% SRF to coal increases the risk of slagging, fouling, and corrosion of the material surface. Particles rich in elemental Ca increase during co-combustion. Blending SRF with MgO-rich coal effectively reduces sintering ash compared to pure SRF combustion.
Click or tap here to enter text.(Prismantoko et al. 2024b)	Coal and RDF	DTF (1250 °C)	5 wt%	The CaO and Cl content of RDF increased the sintering ash of the probe material. Ca-rich agglomerate particles are observed in the RDF ash. After separation into biodegradable and non-biodegradable RDF, two results are observed, 1. sintering ash decreased during co-firing with coal and biodegradable RDF 2. material degradation is observed, particle aggregates increased during co-combustion with coal and non-biodegradable RDF.
(Novendianto et al. 2024)	Coal and RDF	DTF (1250 °C)	5, 10, 15, and 20 wt%	Co-combustion of coal and biodegradable RDF up to 10 wt% showed minimal ash-related problems. The problems increased after 15 wt% biodegradable RDF is added to the coal, as several sintering

References	Fuels	Testing tools	Dosage of waste	Findings
				spots are observed on the probe, ash was dominated by spherical, angular, fine, and Ca-aluminosilicate-rich particles.
(Karuana et al. 2024a)	Coal and SRF	DTF (1200 °C)	5, 10, 15, 20, and 25 wt%	The material degradation increased significantly in the co-combustion of coal and SRF at 15–25 wt%, i.e. more than 50% of the Cr content in SS-304 material is reduced.
(Karuana et al. 2024b)	Coal and RDF	DTF (1250 °C)	10 wt%	The initial degradation of 18Cr-Ni during RDF co-combustion is influenced by the high Cl content of RDF. The Cr content of the material began to degrade in the second hour of operation and increased as the hours of operation increased.
(Ghazidin et al. 2024)	Coal and SRF with additives	DTF (1200 °C)	15 wt%	Ash deposits from co-combustion of 15 wt% SRF are dominated by regular-irregular unfused and sticky particles. The addition of 0.10 wt% additive showed smaller ash particles and reduced sticky particles.
(Ghazidin et al. 2025)	Coal and SRF with additives	DTF (1200 °C)	15 wt%	Ash deposition problems occurred during 15 wt% SRF co-combustion. Some spot sintering is observed on the probe material. The addition of 1.00 wt% Al and Mg type additives can reduce the number of sintering spots during co-combustion.
(Hariana et al. 2025)	Coal and RDF with additives	DTF (1250 °C)	20 wt%	Severe slagging and fouling are observed on co-combustion of 20 wt% biodegradable RDF. Sticky particles were reduced after addition of 1.00 wt% Al-Si based anti-slagging.

Note: SRF: solid recovered fuel; RDF: refused derived fuel; MSW: municipal solid waste; CFB: circulated fluidized bed; DTF: drop tube furnace; HTF: horizontal tube furnace

2. Materials and methods

2.1. Materials properties

Two types of coal, low- and medium-rank coal, were collected from mines in South Sumatera, Indonesia. The selection of low- and medium-rank coal was based on the availability of coal resources which are dominated by low- and medium-rank coal. Both coals were prepared by crushing them to a size of 70 wt% of ≤75 μm to characterize the pulverized-coal-fired (PF) boiler feed particle size. The coals were blended in a 50%:50% ratio by weight and used as the original coal (C100S0) in this experiment. SRF (C0S100) consists of 60% residential garbage, 20% community waste, and 20% garden timber supplied from Tangerang, Indonesia, sorted and dried by bacterial bio-drying. C0S100 was ground and screened to less than 0.8 mm. The samples were characterized according to ASTM standards such as proximate, ultimate, and ash analysis, as summarized in Table 2. Furthermore, C100S0 and C0S100 were blended with proportions of C0S100 (wt% dry basis) in the blends being 5, 10, 15, 20, and 25 wt%, which were coded C95S5, C90S10, C85S15, C80S20, and C75S25, respectively. The SRF dosage variation of 5 wt% up to 25 wt% was chosen to pursue previous research on the impact of various biomasses, including SRF, on ash-related problems in co-combustion applications (Hariana et al. 2023). Compared to C100S0, which has 10 wt% on an air-dried basis, C0S100 has three times higher ash content, with 28.90 wt%. Furthermore, C0S100 has 50-fold higher total chlorine with 0.54 wt% than C100S0 with 0.01 wt%. In addition, C100S0 also has a high total alkali. This affects the blended properties, where the ash content, total chlorine, and alkali content gradually increase as the SRF blending dose increases into the coal, accelerating the ash deposition problem (Zhou et al. 2020). A detailed material analysis can be seen in our previous study (Ghazidin et al. 2023; Prismantoko et al. 2022).

Table 2. Properties of samples

Sample	Proximate Analysis (wt%, adb)				Ultimate Analysis (wt%, adb)					Cl (wt%, adb)
	M	AC	VM	FC	C	H	N	S	O[b]	
C100S0[a]	7.67	9.63	42.44	40.32	60.82	4.49	0.93	0.43	23.70	0.01
C0S100[a]	4.25	28.90	54.19	12.66	33.90	4.25	1.73	0.47	30.75	0.54

[a]: same batch samples with Prismantoko *et al.* (2022); [b]: by difference

Sample	Ash Analysis (wt%)										
	SiO_2	Al_2O_3	Fe_2O_3	CaO	MgO	TiO_2	Na_2O	K_2O	Mn_3O_4	P_2O_5	SO_3
C100S0 [a]	56.41	22.31	6.09	5.70	1.38	0.57	0.64	0.80	0.20	0.13	3.49
C0S100 [a]	33.12	10.80	8.89	20.06	2.28	0.67	0.42	3.60	0.18	3.24	1.99

adb: air-dried basis; M: moisture in a sample; AC: ash content; VM: volatile matter; FC: fixed carbon; C: carbon; H: hydrogen; N: nitrogen; S: sulfur; O: oxygen; Cl: total chlorine

2.2. Thermogravimetric analysis

Thermogravimetric analysis (TGA) was used to assess the thermochemical activity of the fuel. The TGA analysis shows the mass decomposition curve at a set heating rate, including measured temperature parameters such as ignition temperature (T_i) and burnout temperature (T_b). In addition, DTG_{max} indicates the maximum value of mass decomposition at the peak of the mass loss curve. These curves provide a reference basis for determining the impact of SRF blends on coal at combustion characteristics temperature. TGA analyzer Shimadzu DTG-60 series was used to analyze using atmospheric gas of 79% N_2 and 21% O_2 at atmospheric conditions. 5–10 mg of the sample was heated at a 10 °C/min heating rate. The temperature was held for 10 min at 105 °C, then gradually warmed to 900 °C. The temperature set point was 900 °C, based on the typical occurrence of lignocellulosic and polymer materials below 900 °C (Asim et al. 2020; Kan et al. 2016; La Mantia et al. 2017; Pang et al. 2014; Ray and Cooney 2018; Yu et al. 2023).

2.3. Preliminary slagging risk assessment

Ash-related problems were preliminarily assessed using a ternary diagram that has a medium level of accuracy based on a review by Chen et al. (Chen et al. 2021). Vassilev et al. (Vassilev et al. 2013) developed and classified biomass slagging risks based on ash type, hemispherical temperature (HT), and deformation temperature (DT). The ternary diagram, known as the SiO_2–CaO–K_2O (SCK) diagram, was divided into three axes based on material characteristics: $SiO_2 + Al_2O_3 + Fe_2O_3 + Na_2O + TiO_2$ on the right axis, $CaO + MgO + Mn_3O_4$ on the left axis, and $K_2O + P_2O_5 + SO_3 + Cl$ on the bottom axis.

2.4. Ash deposits characterization

Ash deposits were obtained from combustion experiments using a lab-scale drop tube combustor heated to 1200 °C under an air atmosphere to simulate the furnace exit gas temperature of the PF boiler. ~75 g samples per hour were fed into the combustor from the top using a screw feeder. Primary and secondary air rates were regulated to obtain 5% excess oxygen in the flue gas during combustion. A 50 mm diameter uncooled probe equipped with a K-type thermocouple to measure the probe surface temperature was inserted from the bottom of the combustor and adjusted its height until it reached a temperature of 550 °C to represent the metal temperature of the superheater and reheater in the fouling area and 600 °C to represent fireside tube temperature of platen superheater in slagging area. The furnace temperature distribution and detailed schematic diagram of the experiment was provided in Fig. 1. The test was conducted for one hour for each temperature. Ash deposits were collected and separated from the probe by scraping a piece of paper (Hariana et al. 2021). Micro-structure morphology analysis of ash deposits was carried out using Quanta 650 SEM from Thermo Fisher with backscattered and Oxford EDS detectors. X-Act Silicon Drift Detector of EDS detects elements from Be to Pu, with a resolution of 125 eV, following ISO 15632:2002. SEM generates a raster pattern of incident electrons onto the sample surface.

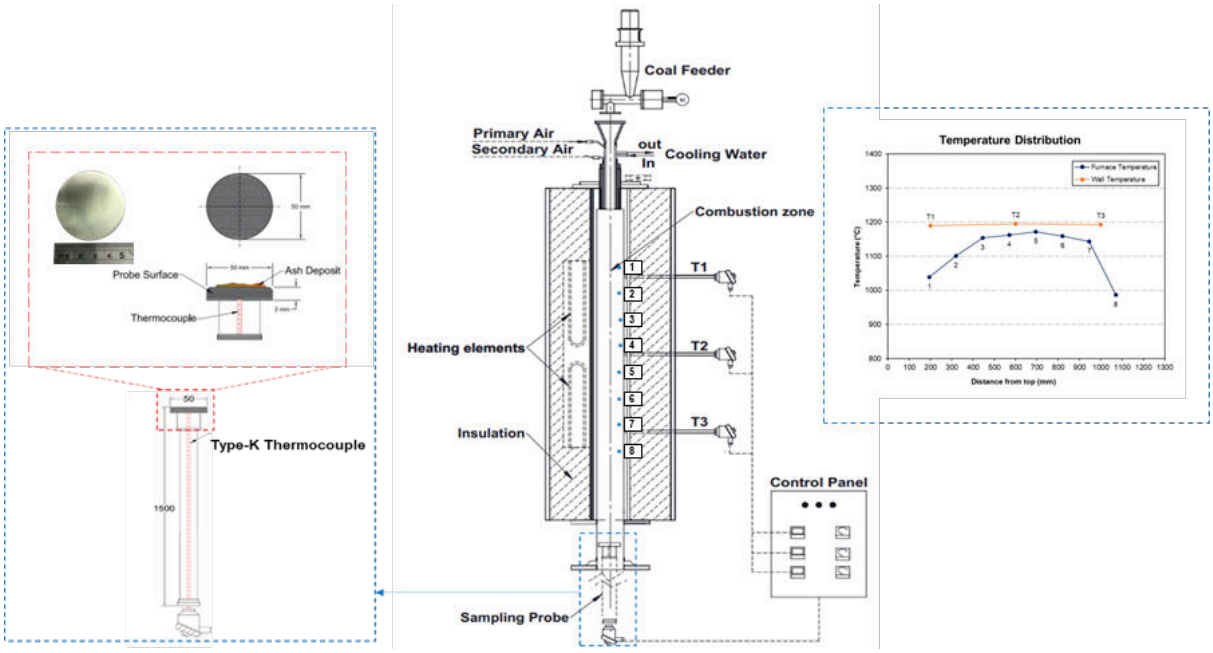


Fig. 1. Schematic diagram of laboratory-scale combustor (modified from (Karuana et al. 2024b))

3. Results

3.1. Thermogravimetry analysis

Combustion characteristics were performed using thermogravimetry analysis. Fig. 2 shows the TG and DTG curves of all tested samples. C0S100, which represents the original SRF sample, demonstrates a markedly disparate ignition and burnout point. C0S100 has the lowest ignition temperature and experiences a deceleration in mass decomposition at temperatures around 300 °C. In contrast, the blended samples show a transition to a decrease in mass rate. C75S25, which initially exhibited the earliest ignition, ultimately became the slowest due to the non-synergistic combustion between biodegradable and non-biodegradable materials in SRF (Gunasee et al. 2016). Meanwhile, C95S5, which is dominated by coal, underwent a gradual decomposition process just prior to the decline in slope similar to the coal sample (C100S0).

A notable discrepancy exists between coal and SRF in terms of burnout conditions. C100S0 entered the burnout phase at 498.16 °C with a residual ash content of 9.64 wt%. The SRF (C0S100) burnout phase commenced at 761.25 °C, leaving an ash residue of 19.21 wt%. This phenomenon may be attributed to the late combustion of non-biodegradable materials present in SRF, resulting in the accumulation of significant quantities of unburned matter (Giraud et al. 2021). The blended samples up to C80S20 exhibited burnout characteristics similar to those of C100S0, indicating that the addition of SRF up to 20 wt% had a minimal impact on combustion. On the other hand, blended samples C75S25 demonstrated higher burnout temperature at combustion with a value of 604.64 °C compared to coal or other blended samples, which have a value of burnout temperature under 500 °C. The greatest quantity of unburned material was observed in C80S20, at 15.99 wt%, and the lowest was C95S5, at 10.79 wt%. The ash content of C75S25 is considered relatively low in comparison to C80S20, due to the synergistic decomposition of carbonaceous material during late combustion (Tejaswini and Pathak 2023).

In the context of combustion reactions, three distinct stages of decomposition are typically observed, namely dehydration, devolatilization, and decarbonization. Based on DTG curves, only C0S100 displays three peaks. The dehydration stage is the stage of free moisture release in the material, which is characterized by a decrease in the mass of the test material since the beginning of heating. In

general, the dehydration stage is represented by the first peak under temperature of 175 °C. The temperature range of the dehydration stage in all test samples is almost similar, but the quantity of decomposed mass looks quite different between the original coal and its blend, as well as the original SRF. As stated in the previous study, C0S100 has the lowest moisture content (Mu et al. 2021). Therefore, the peak mass loss rate in C0S100 has the lowest curve height compared to other samples. The subsequent stage is the breakdown of volatile matter from organic compounds, which is referred to as devolatilization. In general, this process results in the greatest mass loss in comparison to other stages (Tanaka 2016). The volatile matter consists of oxygen-containing groups that are degraded during devolatilization into free radical groups that interact with oxygen to produce lower molecular weight compounds, such as CO and CO_2, in the form of gas (Huang et al. 2022). An increase in the devolatilization temperature results in a shift in the peak position due to the elevated heating temperature (Larionov and Gromov 2019).

Meanwhile, the DTG value is observed to be unstable, exhibiting both increasing and decreasing trends, influenced by the shift in ignition temperature and burnout sample in line with the addition of SRF to coal (Ma et al. 2006). The C100S0 sample exhibits the highest decomposition peak among the various sample types, with a value of 17.94 %/min at 334.82 °C. In contrast, C0S100 exhibits the lowest decomposition peak, with a value of 8.62 %/min. High ash content in C0S100 affects oxygen diffusion and reduces the heat transfer rate, which results in a slower burning rate (Das et al. 2021).

The final stage of decomposition is designated as decarbonization, which is exclusively manifested in C0S100 as an indication that the sample is still undergoing cracking under elevated temperature conditions. In comparison to coal and blended samples, C0S100 exhibits a late combustion process, resulting from the combustion of residual carbon present in the inorganic material (Sun et al. 2021; Zhu et al. 2024).

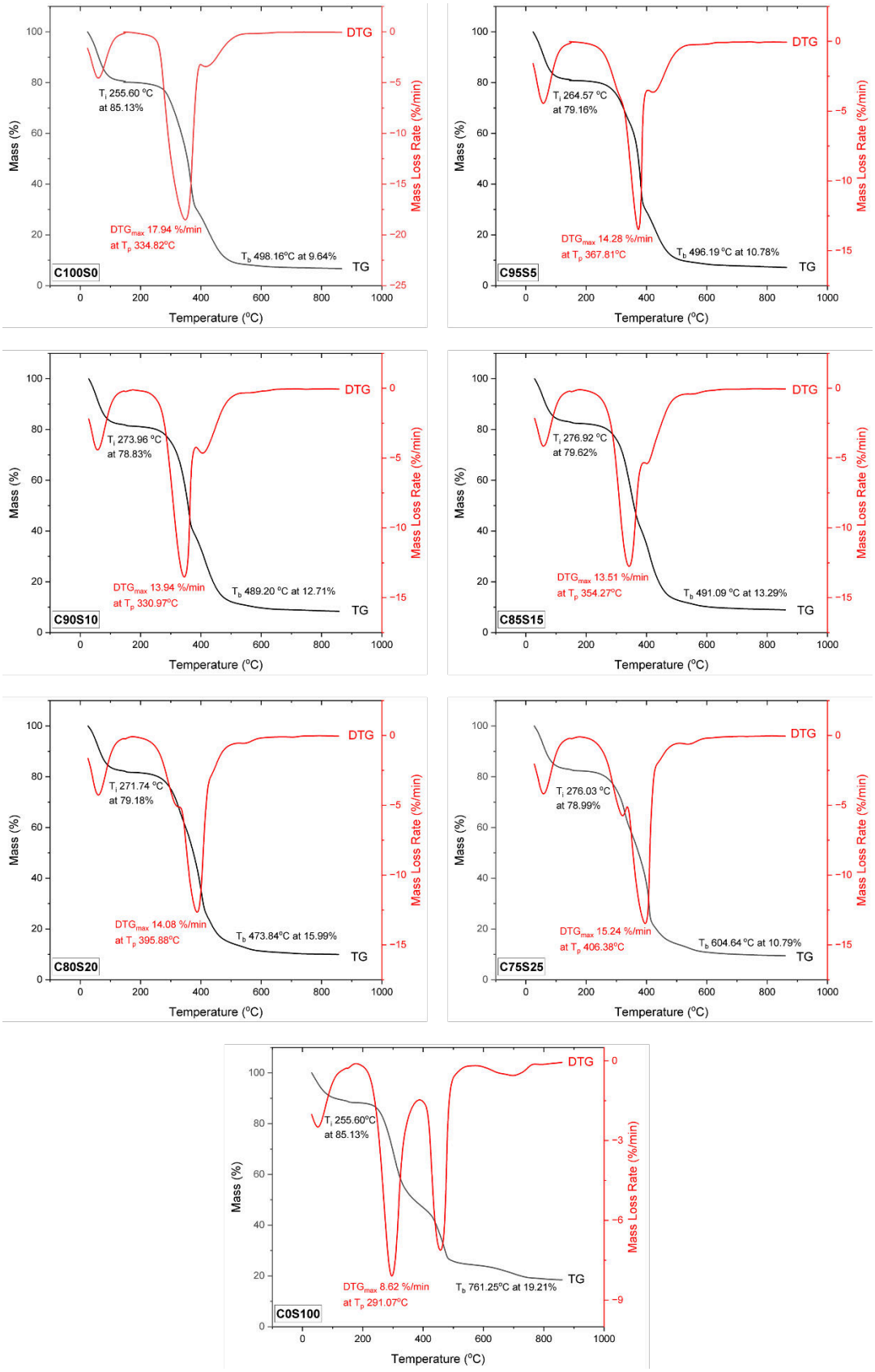
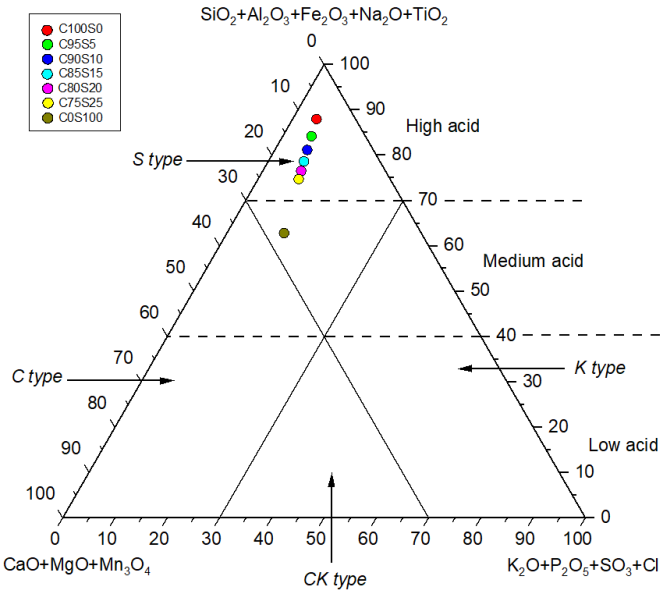


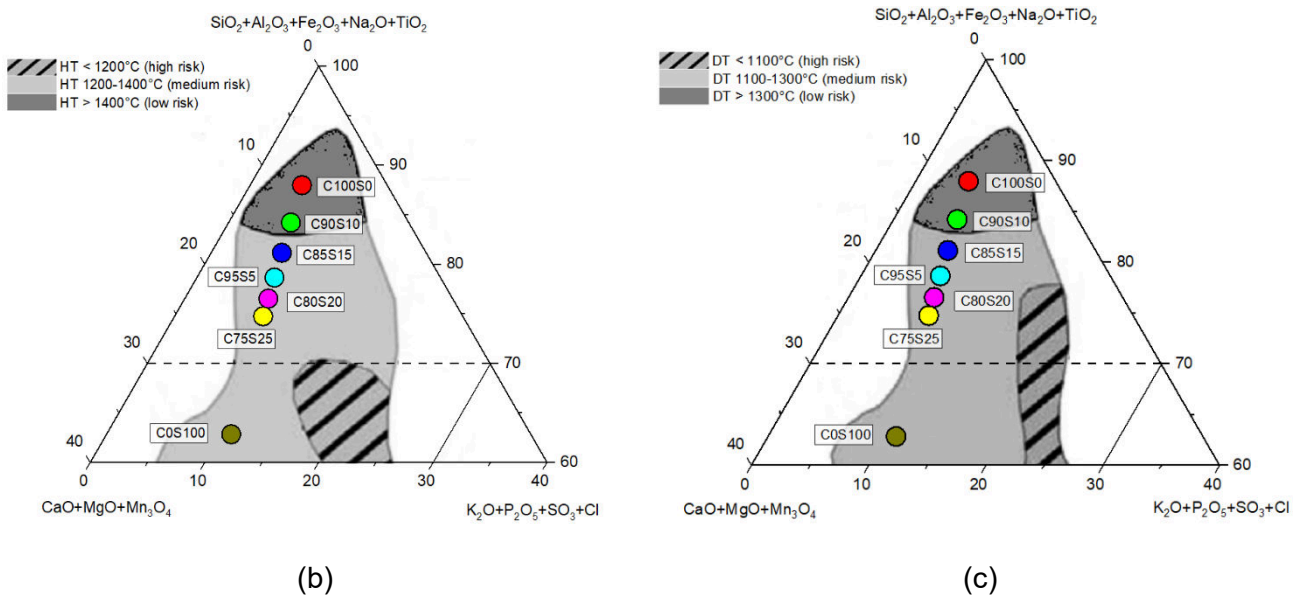
Fig. 2. TG and DTG curves of coal, SRF, and the blended

3.2. Preliminary ash deposition risk assessment

A preliminary study using the SCK ternary diagram method was conducted to estimate the slagging risk of the tested samples based on ash properties and ash fusion temperature area. Ash types are classified into four types (S, C, K, and CK) while acid types are classified as low acid (LA), medium acid (MA), and high acid (HA). To estimate the risk of slagging, a categorization based on HT and DT areas was applied, which was developed by Vassilev et al. (Vassilev et al. 2014) using 60 different biomass types for HT areas and 55 different biomass types for DT areas. Based on the SCK ternary diagram of the tested sample presented in Fig. 3, it is shown that all tested samples are categorized as S-HA (S-type high acid) except C0S100, which is at S-MA (S-type medium acid). The dominance of SiO_2, Al_2O_3, and Fe_2O_3 elements make the samples categorized as S-type. Type S with high potassium content is expected to have a high risk of slagging, while high acidity has a higher corrosion risk (García et al. 2015). In comparison with other separate studies, SRF falls into the same category as potassium-rich switchgrass (Vassilev et al. 2014), while coal is generally categorized as S-HA (Ghazidin et al. 2024; Prismantoko et al. 2024a; Suyatno et al. 2023; Vassilev et al. 2014). Meanwhile, based on the HT and DT areas, C100S0 and C90S10 have a low risk of slagging by being in the HT > 1400 °C and DT > 1300 °C areas. Meanwhile, C0S100 and other mixtures have a medium slagging risk when entering the HT and DT areas, 1200–1400 and 1100–1300 °C, respectively.



(a)



(b) (c)

Fig. 2. Slagging risk estimation adopted from Vassilev et al. (Vassilev et al. 2014); (a) SCK diagram; (b) HT area; (c) DT area

3.3. Ash deposits characterization

3.3.1. C100S0 ash deposits

Fig. 4 presents the backscattered electron (BSE) images and elemental composition of the C100S0 ash deposits at two probe temperatures. When observed in its entirety, C100S0 ash deposits are tiny particles less than 100 µm in size, most of which are unmelted and irregular. At the 550 °C of the probe, as shown in Fig. 4 (a), structures of unmolten solid spheres and amorphous irregular particles indicated quartz minerals' dominance in the deposits. This phenomenon indicates that these particles do not experience melting during combustion. Based on the EDS results, the composition of C100S0 ash deposits was mainly Si, Al, and Fe with smaller amounts of Ca, Mg, and S. The distribution of these elements indicates that aluminosilicate elements dominate the ash deposit with small dispersed elements. At 300× magnification, Ca-rich fine particles such as those in spot 1 promote the reaction of CaO with sulfur in coal ash to form anhydrite, as shown in Reaction (1) (Vassilev et al. 2013). Despite having a melting temperature above 1200 °C, at temperatures of 800–1300 °C, anhydrite can release sulfur into the flue gas.

$$CaO + SO_3 \rightarrow CaSO_4 \quad (1)$$

Meanwhile, coarse particles of 5–10 μm in spots 2, 3, and 6 are dominated by Fe and may form hematite during combustion. The occurrence of hematite must be considered, as it can interact with alkalis to produce low melting point minerals (Vassilev et al. 2013; Werther et al. 2000). At spots 4 and 5, smooth and coarse-sharply irregular quartz is indicated with aluminosilicate dominating the particle composition, with minor elements of Ca, K, and S. Due to their high melting temperature, these irregular particles maintain their shape during combustion, consistent with that reported by Li et al. (Li et al. 2016). Identical to those at the 550 °C temperature, at 600 °C, element composition generally shows the dominance of Si, Al, Fe, and Ca with irregular amorphous shapes particles (Fig. 4 (b)). No melted solid ash formed on the probe surface due to the low alkali and sulfur content. However, fine irregular Ca-rich melts are also present at this 600 °C probe, for example, at area B. Specifically, at spot 1, SiO_2-rich quartz material, the main coal ash mineral, was observed. Coarse irregular particles <50 μm in size containing Si, Ca, and Al found in spots 3 and 5 indicate the presence of an anhydrite mineral in the deposit. While at spots 2, 4, and 6, the coarse white structure indicates hematite minerals with the dominance of Fe. From the results of morphology and elemental composition, the origin C100S0 appears clean with no significant melting or slagging attached to the probe surface, supported by the presence of high melting elements in the ash deposit. This result is consistent with the investigation in our previous work, which showed that the coal used in this study has no possibility of slagging based on visual observation (Prismantoko et al. 2022).

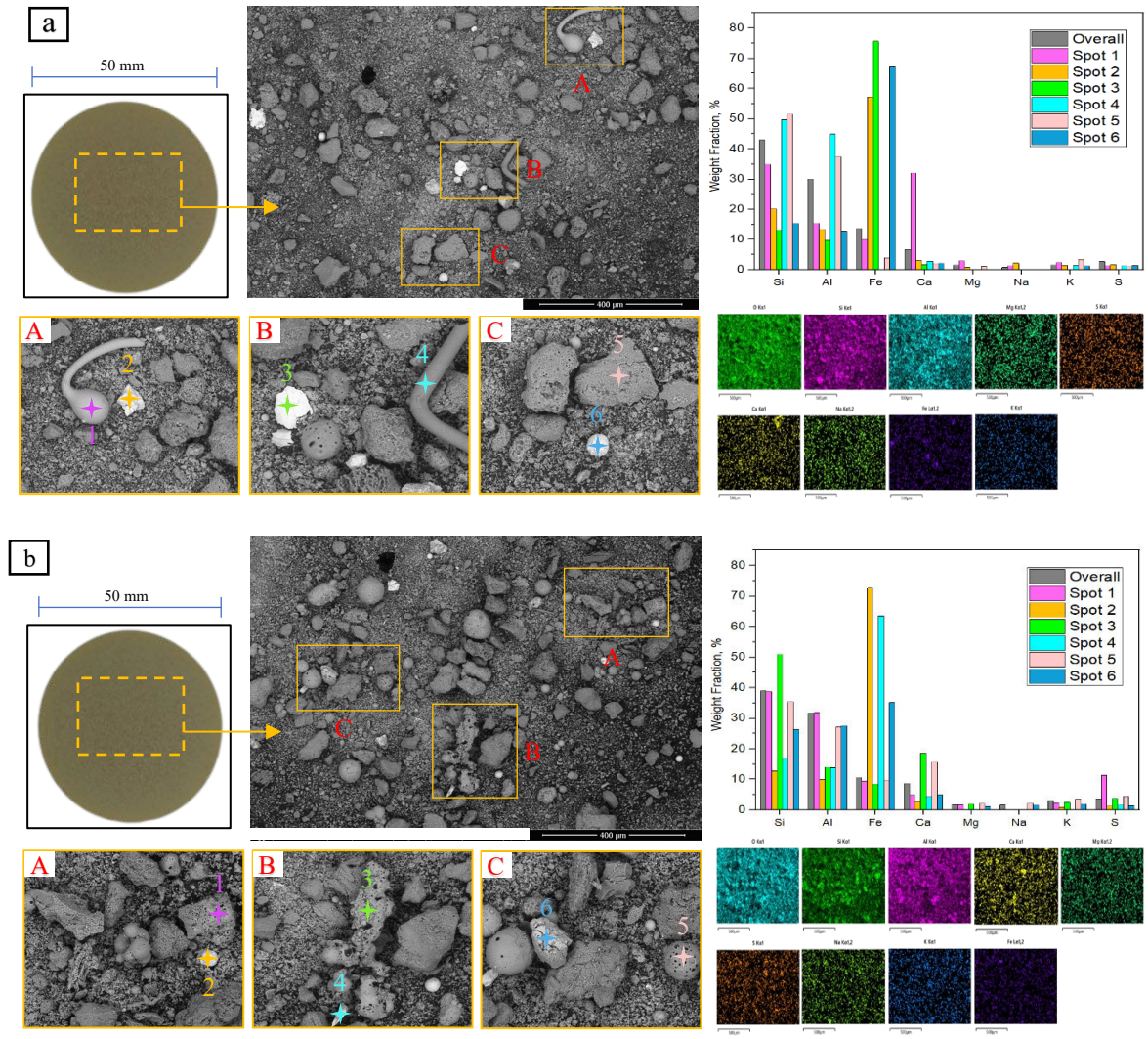


Fig. 4. BSE image with elements of C100S0 ash at the probe temperature of (a) 550 °C; (b) 600 °C

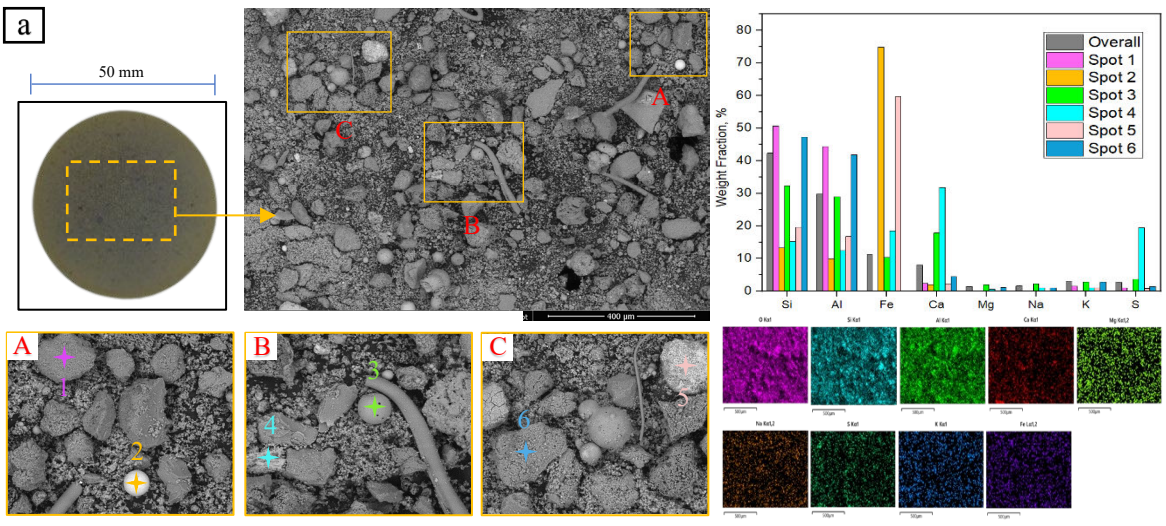
3.3.2. C95S5 ash deposits

SEM-EDS at selected spots of C95S5 ash deposits is shown in Fig. 5. Particles less than 100 μm in the form of unmolten solid spheres and amorphous irregular particles still dominate the deposits. EDS results show that Si, Al, Fe, and Ca dominate the ash with minor Mg, Na, and K. At 550 °C, as shown in Fig. 5 (a), with the addition of 5 wt% SRF to the coal, the ash deposits are dominated by Si and Al with minor Fe and Ca. When amplified at 300×, spots 1 and 6 showed amorphous irregular particles with a size smaller than 100 μm, mainly dominated by aluminosilicate. Moreover, white Fe-rich particles are also observed in C95S5 ash, for example, in spots 2 and 5, which promote the formation of Fe_2O_3 minerals in the ash. In addition, smooth spherical particles less than 10 μm in size

appear to form in several spots, including spot 3, indicating that these particles were fully molten during combustion. Spot 3, which is dominated by Si and Al-rich particles with Ca at 17,85 wt%, suggests the presence of Ca-aluminosilicate in the deposits and forms the mineral anorthite at 800–1000 °C with a lower melting point than quartz in the original coal. The reaction between SiO_2, Al_2O_3, and CaO is represented in Reaction (2) (Vassilev et al. 2013; Zhang et al. 2023). Irregular grey fibrous particles rich in Ca and S, possibly forming the mineral anhydrite with a relatively low melting point, were observed at spot 4.

In contrast, at 600 °C (see Fig. 5 (b)), medium-sized particles in the form of high-melting irregular particles dominated by Si, and Al were found in the ash, which is observed in almost all areas (e.g., spots 1, 2, 3, 4, and 5). It indicates that quartz formation dominates at this temperature. Meanwhile, fine spherical particles rich in Ca, Fe, and S are evident, promoting the formation of hematite or anhydrite. Overall, increasing the temperature and adding SRF to the coal causes the particle size to increase, and the fused particles are more visible. In addition, with the increase of Ca content in the ash deposit, the reaction between Si, Al, and Ca increases and promotes the formation of anorthite, which is not seen in the original coal ash deposit. However, the morphology shows an insignificant melting phenomenon in the co-combustion of 5 wt% SRF and coal.

$$CaO + Al_2O_3 + 2SiO_2 \rightarrow CaAl_2Si_2O_8 \quad (2)$$



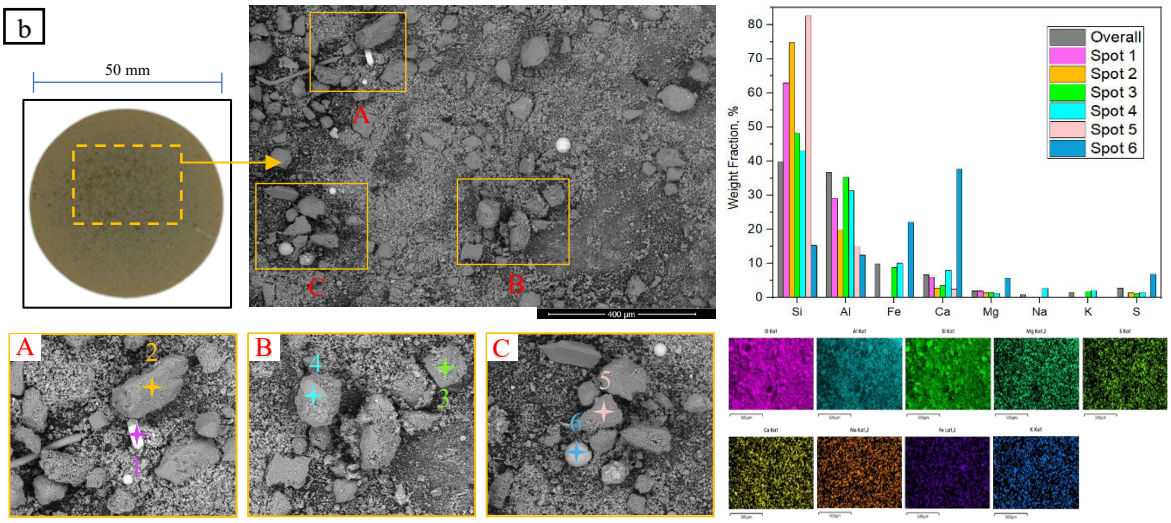


Fig. 5. BSE image with elements of C95S5 ash at the probe temperature of (a) 550 °C; (b) 600 °C

3.3.3. C90S10 ash deposits

Fig. 6 shows the SEM image and elemental maps with EDS results of the whole and selected spots of the C90S10 ash deposit. Smooth and irregular particles rich in Si-Al with fine agglomeration particle size below 100 µm were found in the deposit. Fig. 6 (a) shows the SEM image and EDS at a temperature probe of 550 °C. For the areas selected, spots 1, 3, 4, and 5 of temperature 550 °C with 300× magnification, coarse-irregular particles of about 50–100 µm composed of aluminosilicate were observed in the deposit. While at spot 2 Ca-rich smooth irregular particles and at point 6 spherical smooth particles with a size of 10 µm were observed. Based on the EDS result, the ash deposit at spots 2 and 6 mainly comprises Ca, Al, Si, and S, forming anorthite or anhydrite. At 600 °C, as shown in Fig. 6 (b), at spots 1 and 6, white particles containing hematite of above 10 µm in size were found. In addition, in spots 2 and 3, coarse particles with Si composition show that slagging is unlikely to happen. Meanwhile, the Si, Al, Ca, and S-rich particles are fused smooth particles seen in spots 4 and 5. Based on the identical shape and EDS results of the C90S10 ash deposits at both temperatures, the chance of forming slagging and fouling is insignificant.

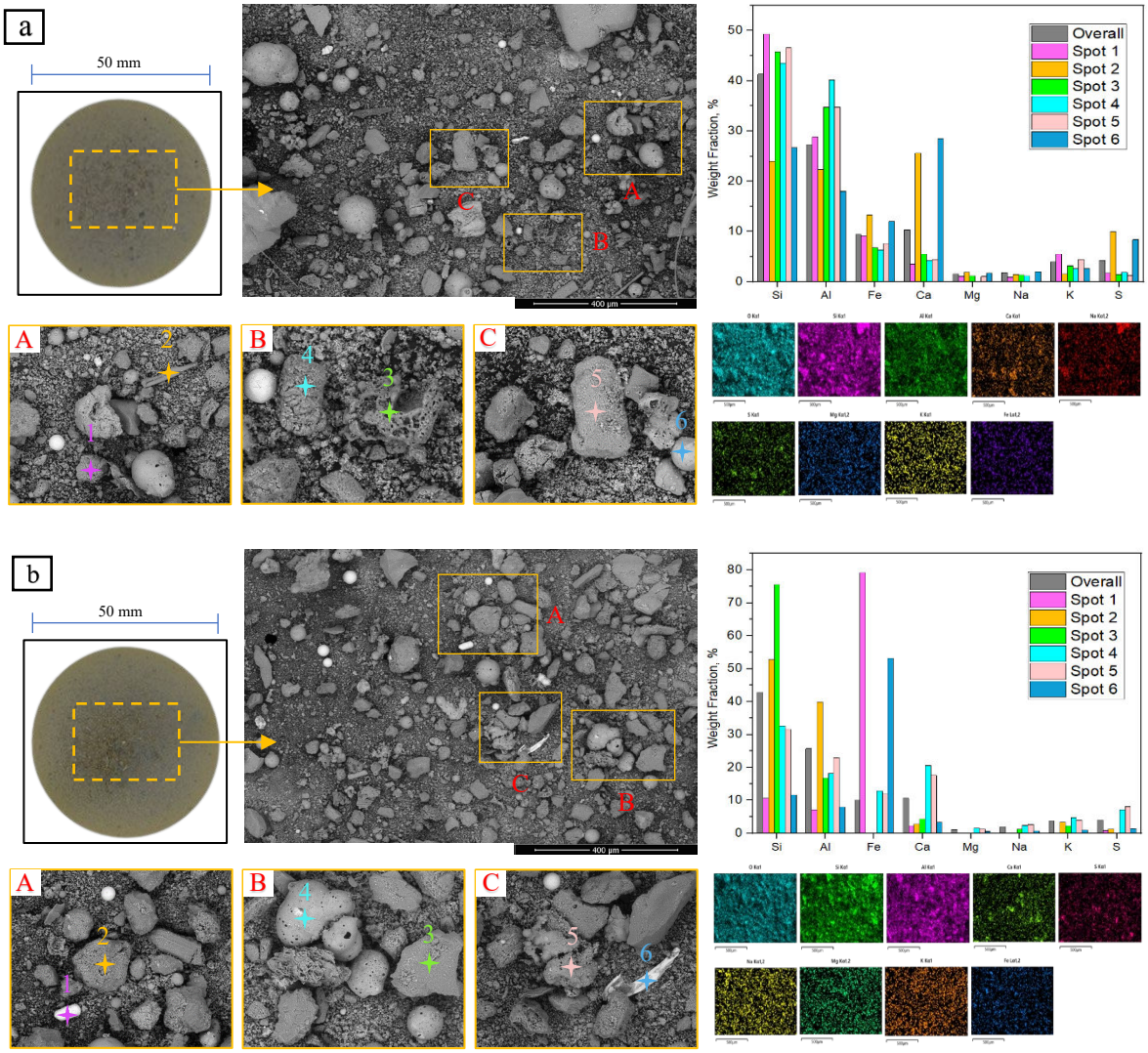


Fig. 6. BSE image with elements of C90S10 ash at the probe temperature of (a) 550 °C; (b) 600 °C

3.3.4. C85S15 ash deposits

Fig. 7 depicts the BSE image with elemental maps and the composition of the C85S15 ash deposit. In general, although Si-Al elements are still dominant in this ash deposit, fine and fused particles rich in Fe and Ca begin to dominate in the C85S15 ash deposit. The anorthite mineral initiated by the presence of Ca increases. It will increase the risk of slagging and fouling. With 300× magnification, spot 1 at 550 °C, shown in Fig. 7 (a), shows fine rod-shaped Si and Al particles. Moreover, particles that Si-Al mainly dominate with high addition of Ca and S are found in spots 2, 4, and 6. Anorthite or anhydrite probably formed at this spot. At the same time, the Fe-rich particles are surrounded by smooth and fused particles, as in spots 3 and 5. Similar to 550 °C, at the probe temperature of 600 °C as shown

in Fig. 7 (b), it generally consists of Si, Al, Fe, and Ca. Spots 1, 3, 4, and 5 show fine particles with a size of 100 µm rich in calcium oxide that forms the mineral anorthite as it interacts with Si and Al or anhydrite as it interacts with sulfur, which has a lower melting point than quartz. However, quartz particles are still detected in spot 2. Spot 6 shows white particles rich in Fe. In addition, tiny-fused particles spread in the ash deposit indicate that the slagging phenomenon is starting to occur.

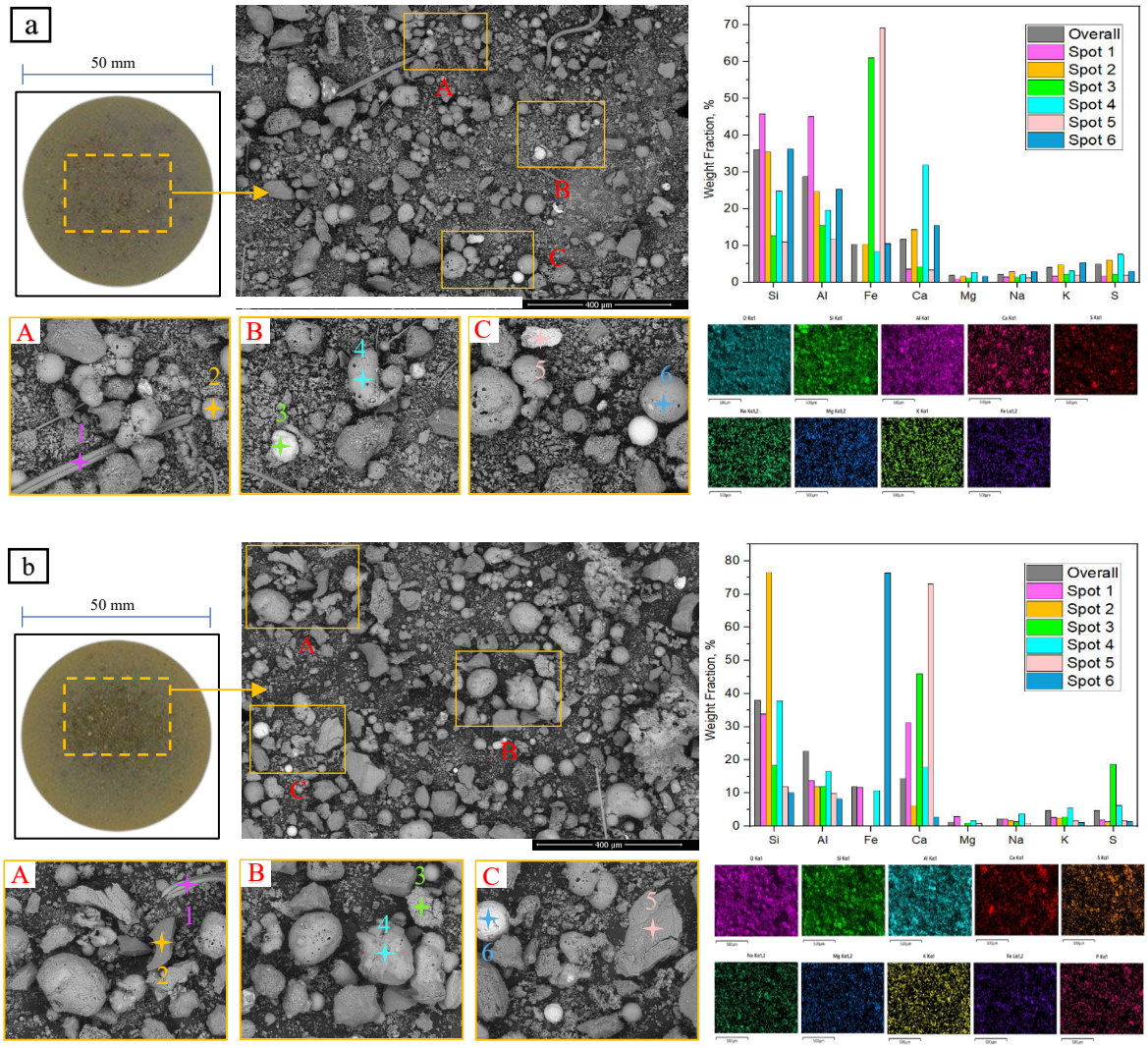


Fig. 7. BSE image with elements of C85S15 ash at a temperature of (a) 550 °C; (b) 600 °C

3.3.5. C80S20 ash deposits

The morphology and elemental composition of the C80S20 ash deposit are illustrated in Fig. 8. Similar to the observation of C85S15, the ash deposits are dominated by irregular-smooth, molten, and fused particles with Si, Al, Fe, and Ca-rich composition. In more detail, at 550 °C, shown in Fig. 8 (a),

spots 1, 4, and 5 show that coarse particles in the form of quartz are still present in the ash deposit. Particles containing Si, Al, and Ca below 100 µm were found in spots 2 and 6. In addition, there are also Fe-rich particles, as shown in spot 3. However, irregular and molten particles appear widely distributed in several spots. In contrast, at 600 °C (see Fig. 8 (b)), particles with a size of more than 100 µm in the form of Ca-rich fine spherical particles, as shown in spots 1, 3, and 5, are particles that have experienced melting. Fe-rich particles are still present, indicated by white particles in spot 4. In addition, quartz particles were found in spot 2. Furthermore, larger particle sizes and more melted particles were found in the 20 wt% SRF blend. These findings confirm that a higher portion of SRF will increase the potential for slagging and fouling.

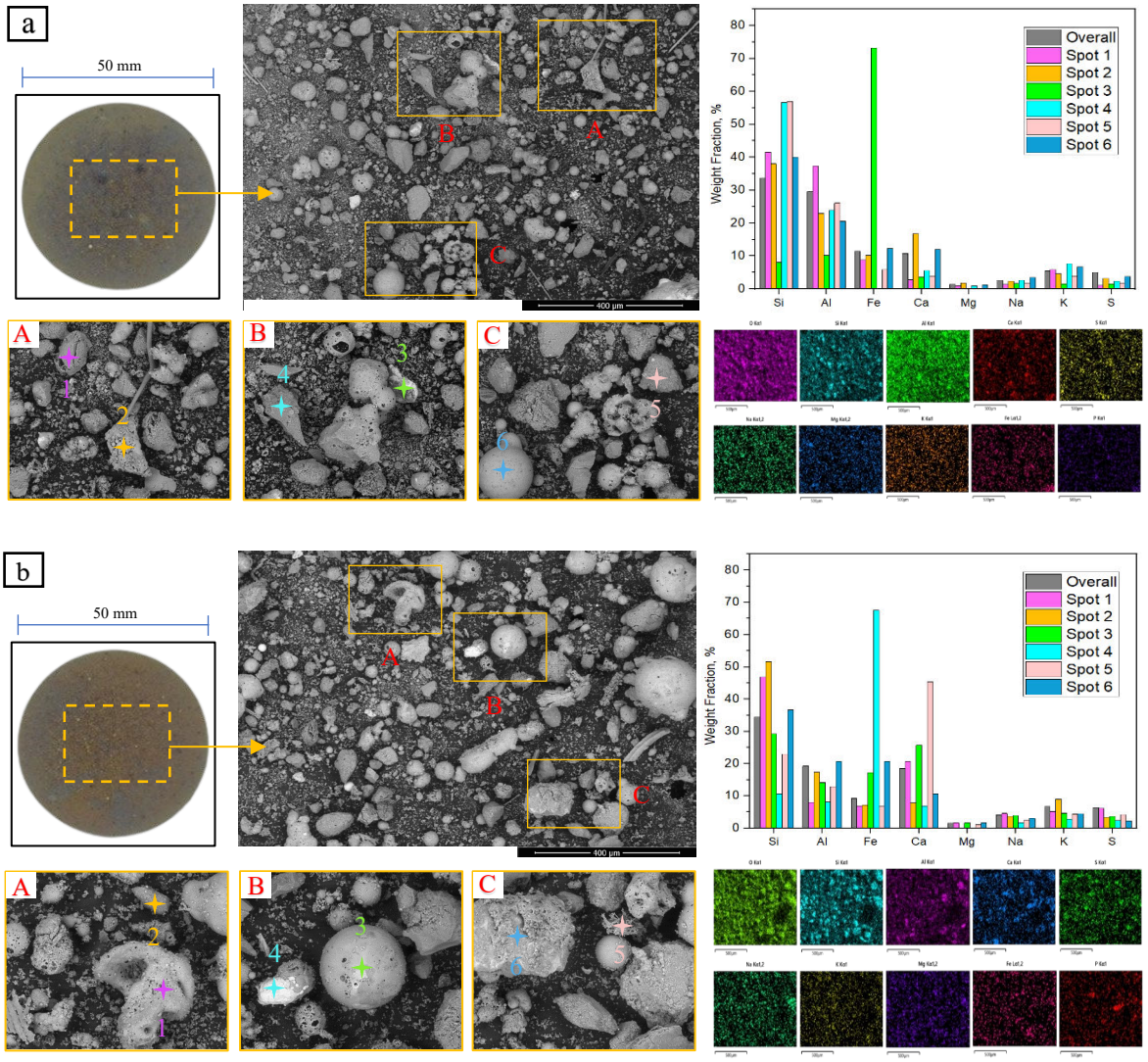
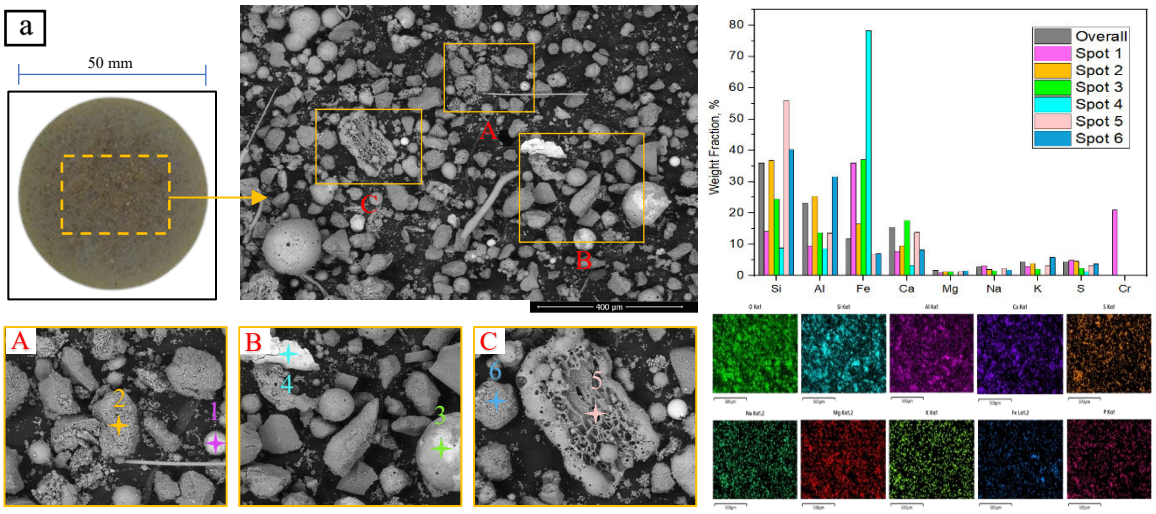


Fig. 8. BSE image with elements of C80S20 ash at the probe temperature of (a) 550 °C; (b) 600 °C

3.3.6. C75S25 ash deposits

The BSE image with the EDS result of the C75S25 ash deposit are depicted in Fig. 9. C75S25 ash deposits are dominated by irregular-coarse, molten spherical, and agglomerate particles below 100 µm in size, indicated by the formation of sodium silicate. EDS results show that the C75S25 ash deposits mainly comprised Si and Ca, with minor Na, K, and S condensed on the surface. Alkali and sulfur contents were found in all spots at both temperatures. Higher Ca/Si content on C75S25 promotes K release, easily forming potassium sulfate or potassium chloride (Xue et al. 2017). Fig. 9 (a) illustrates the morphology and elements at 550 °C. At points 1, 3, and 4, particles with high Fe content were found in the ash. Large irregular coarse containing SiO_2 indicate the presence of unmelted particles at point 5. Si-Al-rich coarse particles were also found in spots 2 and 6. However, some fine spherical particles easily melt in other spots. Meanwhile, irregular coarse particles rich in Si and Al were found at points 1 and 6 at 600 °C, as shown in Fig. 9 (b). In addition, spots 2, 4, and 5 are irregular fused particles containing Si, Al, Ca, K, and S. This increases K-aluminosilicate formation.

Moreover, Fe-rich particles at spot 3 in the form of hematite were found. However, Cr is present in the ash at point 3 at 18.72 wt%. The presence of Cr increases the occurrence of corrosion during combustion. Metals containing Cr and Fe at 425–525 °C start to corrode (Liu et al. 2014). At spot 2, irregular sharp crystals rich in Si and O with minor Ca and alkali-sulfur contents were found. In addition, several spots with small-sized melted particles are scattered in the ash deposit.



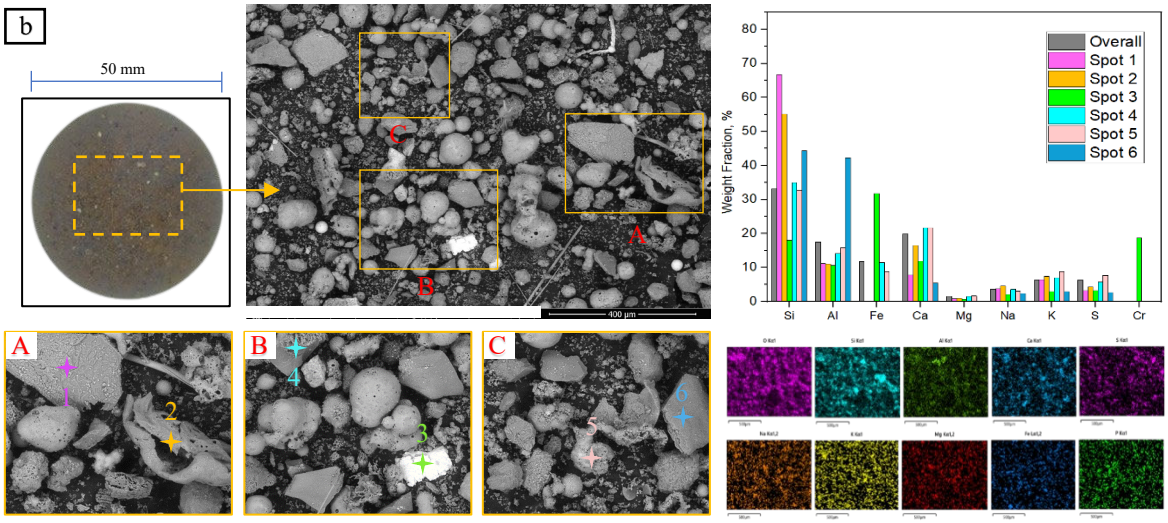


Fig. 9. BSE image with elements of C75S25 ash at a temperature of (a) 550 °C; (b) 600 °C

3.3.7. C0S100 ash deposits

The C0S100 ash deposit, which is 100 wt% SRF combustion ash, is mostly agglomerated fine particles with a size of 50–300 µm, as shown in Fig. 10. The EDS results show that Ca, Fe, Na, and K dominate at both probe temperatures with the presence of Cl in the ash. In spots 1 and 3 at 550 °C, as shown in Fig. 10 (a), the fine particles are dominated by Fe and Ca above 20 wt%. Fe and Ca will react with alkali vapor, which can accelerate slagging. In spots 2, 4, 5, and 6, the element Ca is more dominant by forming a low melting point mineral, albite. In addition, alkaline elements and Cl were found to be quite high in the C0S100 ash deposit. At 600 °C, as shown in Fig. 10 (b), high K and Si elements are found in spot 1.

Furthermore, spot 3 is dominated by K and Cl elements at 41.39 wt% and 37.75 wt%, respectively. K and Cl will form KCl and then react with SiO_2 or $CaSO_4$ to form $K_2Si_2O_5$ or K_2SO_4. Alkaline sulfate easily condenses and then promotes fouling on the probe surface (Liu et al. 2019). On the other hand, in spots 2 and 5, smooth particles containing high Ca were found, which will form the mineral albite when it meets alkali and silica oxide. Albite with a low melting temperature of about 1118 °C, possibly formed via the reaction of Na_2O, Al_2O_3, and SiO_2 at temperatures above 575 °C, as shown in Reaction (3) (Vassilev et al. 2013; Zhang et al. 2023). Spot 4 is Al and Ca-rich particles forming the mineral anorthite. Meanwhile, white particles of Fe were found in spot 6. Cr was also found in this spot,

indicating corrosion-affected material with the formation of alkaline chloride, as shown in Reaction (4) (Karuana et al. 2024b). Alkaline chloride (K_2CrO_4) more easily degrades metal materials than alkali sulfate (Pettersson et al. 2008). With various minerals and elements with low melting points and the formation of sticky agglomerated fine particles, C0S100 is not recommended for single firing.

$$Na_2O + Al_2O_3 + 6SiO_2 \rightarrow 2NaAlSi_3O_8 \quad (3)$$

$$½Cr_2O_{3(s)} + 2KCl_{(s)} + 5/4O_{2(g)} \rightarrow K_2CrO_{4(s)} + Cl_{2(g)} \quad (4)$$

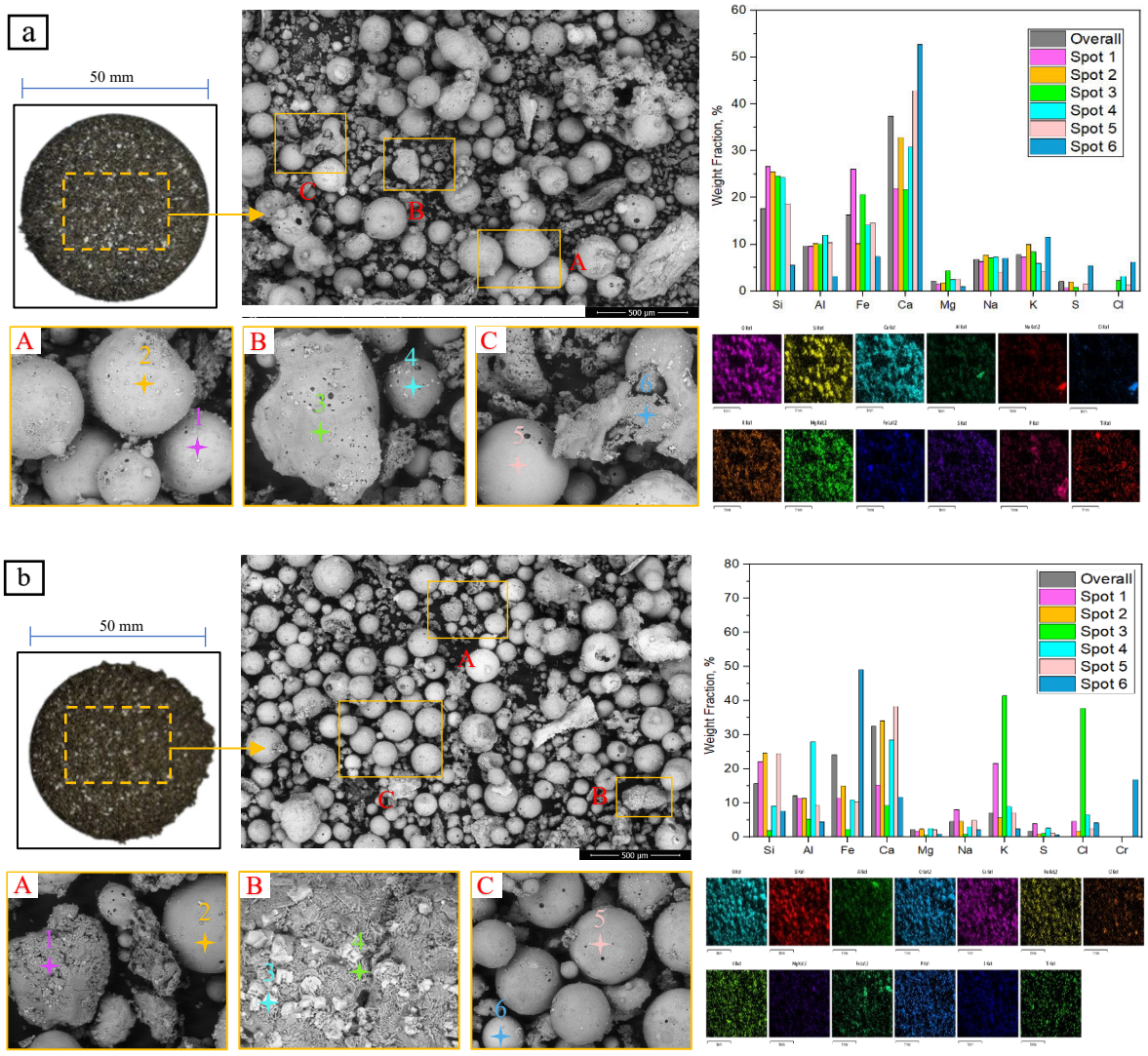


Fig. 10. BSE image with elements of C0S100 ash at a temperature of (a) 550 °C; (b) 600 °C

4. Overall Summary

Combustion performance using thermogravimetry analysis, preliminary slagging risk assessment, and the morphology of ash deposits formed at probe surface temperatures of 550 and 600 °C during co-combustion of coal and solid recovered fuel were comprehensively characterized. Findings related to combustion characteristics studies show that the incorporation of SRF into the coal mixture results in a shift in the ignition temperature profile towards reduced temperatures, accompanied by an increase in mass loss. This phenomenon can be attributed to the fact that SRF is predominantly composed of inorganic matter, which is more readily ignitable at lower temperatures. However, it is known that SRF has late combustion characteristics, which extend the burnout temperature profile and may result in unburned material deposition. Furthermore, the addition of SRF to the material has been observed to decrease its reactivity, as evidenced by a reduction in the DTG_{max} value with each addition of SRF to coal, with the exception of sample C75S25. Based on the preliminary estimation of slagging risk using the SCK ternary diagram method, coal has a low slagging risk, while SRF and blends have a medium risk, except for blends with a 10 wt% SRF ratio, which have a low slagging risk.

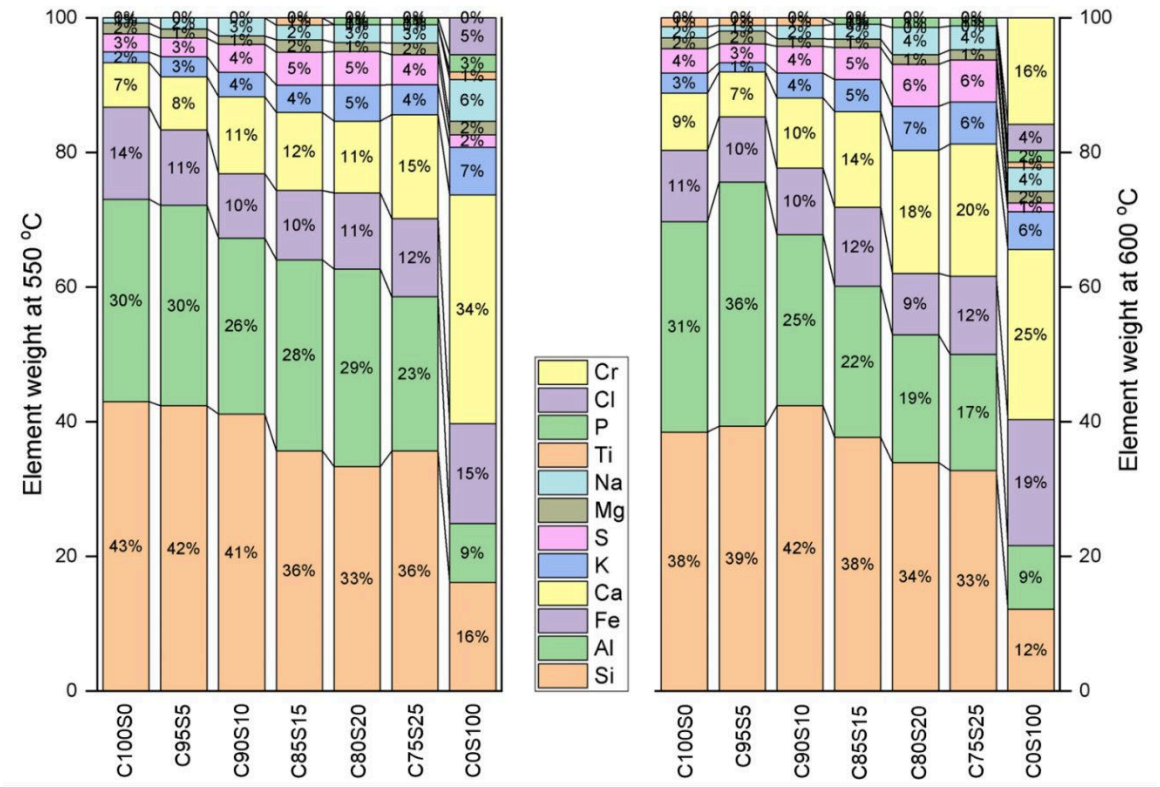


Fig. 11. Elemental composition comparison of ash deposits of tested samples

Furthermore, based on ash characteristics, backscattered electron images of the samples show that the particle size varies, ranging from less than 10 μm to 300 μm. The main ash structures are solid, coarse, agglomerated, irregular, and unburned carbon particles dominated by elements Si, Al, Fe, and Ca. Agglomerated particles rich in alkali and sulfur were also observed and became more obvious as the percentage of SRF in the blends increased. The C100S0 ash deposit is dominated by unmolten solid spheres and amorphous irregular particles with Si element, where the ash deposits at both probe temperatures are dominated by high melting quartz. This result indicates that no slagging phenomenon occurs in C100S0 combustion. In contrast, at C0S100, sticky and low melting point particles dominate the ash deposit. Alkali and chlorine content in SRF lead to ash sintering and corrosion of the probe surface. Moreover, with SRF blends to coal, the alkali, calcium, magnesium, and sulfur in SRF will precipitate on the probe material during combustion and accelerate slagging-fouling. In the 5–10 wt% blend, SEM results still show quartz elements and particles dominating despite the decreasing composition. Particles containing lower melting point mineral-forming elements begin to dominate at C85S15 and C80S20 with 15–20 wt% SRF blends, initiating ash deposition. The peak occurs at C75S25, where the ash melt phenomenon is observed. Large particles with low melting points start to adhere to each other, where C75S25 is dominated by Ca-aluminosilicate. Based on the elemental composition comparison of all tested samples shown in Fig.11, by adding SRF to coal, refractory elements such as Si and Al decrease while fluxing elements such as Ca, Na, K, and S rise which leads to a lower AFT value (Vassilev et al. 2014). Finally, adding more SRF to the coal can lower the ash fusion temperature and accelerate slagging and fouling. Table 3 shows an overview of the summary of study results.

Table 3. Summary of study overview

Sample	Slagging risk estimation by SCK diagram	Thermogravimetry analysis		Ash Characterization		Description
C100S0	Slagging risk is low (HT > 1400 °C and DT > 1300 °C) and	T_i T_b DTG_{max}	255.60 °C at 85.13% 498.16 °C at 9.64% 17.94 %/min at T_p 334.82 °C	550 °C 600 °C	<50 μm fine, unmolten, and irregular particles rich in Si and Al with Fe found in some spots	Low-risk coals high in Si and Al show a predominance of particles with high melting points.

	categorized as S-type high acid				<100 µm fine, unmolten, and irregular particles rich in Si, Al, and Fe	
C95S5	Slagging risk is medium (HT 1200–1400 °C and DT 1100–1300 °C) and categorized as S-type high acid	T_i T_b DTG_{max}	264.57 °C at 79.16% 496.19 °C at 10.78% 14.28 %/min at T_p 367.81 °C	550 °C 600 °C	<100 µm unmolten solid spheres and irregular particles rich in Si, Al, Fe, and Ca <70 µm fine, unmolten spheres and irregular particles rich in Si, Al, Fe, and Ca	It has combustion performance and ash characteristics similar to coal. The increase in Ca content is a response to the addition of SRF to the coal.
C90S10	Slagging risk is low (HT > 1400 °C and DT > 1300 °C) and categorized as S-type high acid	T_i T_b DTG_{max}	273.96 °C at 78.83% 489.20 °C at 12.71% 13.94 %/min at T_p 330.97 °C	550 °C 600 °C	<100 µm smooth and irregular particles with few fine agglomerations rich in Si and Al with Fe and Ca found in some spots <100 µm smooth, irregular, and fine agglomeration particles rich in Si, Al, Fe, and Ca	Low risk of slagging based on preliminary estimates, but small agglomerated particles are starting to be observed, albeit in small quantities.
C85S15	Slagging risk is medium (HT 1200–1400 °C and DT 1100–1300 °C) and categorized as S-type high acid	T_i T_b DTG_{max}	276.92 °C at 79.62% 491.09 °C at 13.29% 13.51 %/min at T_p 354.27 °C	550 °C 600 °C	<100 µm molten, fine, and fused particles rich in Si, Al, Fe, and Ca <300 µm smooth, molten, and fused particles rich in Si, Al, Fe, and Ca with minor S	Ca-rich particles dominate particle agglomeration increases. Preliminary estimates based on SCK also indicate a moderate risk.
C80S20	Slagging risk is medium (HT 1200 – 1400 °C and DT 1100 – 1300 °C) and categorized as S-type high acid	T_i T_b DTG_{max}	271.74 °C at 79.18% 473.84 °C at 15.99% 14.08 %/min at T_p 395.88 °C	550 °C 600 °C	<100 µm molten and fused particles rich in Si, Al, Fe, and Ca 10–200 µm irregular-smooth, molten, and fused particles rich in Si, Al, Fe, Ca, K, and S	The combustion characteristics are still identical to coal, but the dominance of Ca- and K-rich molten particles was observed from the ash deposition characteristics.
C75S25	Slagging risk is medium (HT 1200–1400 °C and DT 1100–1300 °C) and categorized as S-type high acid	T_i T_b DTG_{max}	276.03 °C at 78.99% 604.64 °C at 10.79% 15.24 %/min at T_p 406.38 °C	550 °C 600 °C	≤100 µm molten smooth and agglomerate particles rich in Si, Al, Ca, and Fe 10–200 µm irregular-coarse, molten, and agglomerate particles rich in Si, Al, Ca, and Fe with the presence of Cr	The burnout temperature began to increase at this ratio due to the high ash content. In addition, Cr-containing particles began to be observed in several spots, indicating the occurrence of material degradation.
C0S100	Slagging risk is medium (HT 1200–1400 °C and DT 1100–1300 °C) and categorized as S-type medium acid	T_i T_b DTG_{max}	255.60 °C at 85.13% 761.25 °C at 19.21% 8.62 %/min at T_p 291.07 °C	550 °C 600 °C	50–300 µm agglomerated fine particles rich in Ca, Fe, Na, and K <300 µm agglomerated fine particles rich in Ca, Fe, Na, and K with the presence of Cl and Cr	The morphological results align with the sample characterization results where high Ca, K, and Cl in the sample increase the risk of ash deposition and corrosion.

5. Conclusions

From a series of assessments, analyses, and observations that have been carried out, three important findings were obtained, including:

1. According to thermogravimetry analysis, the addition of up to 20 wt% SRF has a minor effect on the ignition and combustion rate of coal. However, at 25 wt% SRF starts to raise the burnout temperature by ~150 °C to 604.64 °C at 10.79% due to the high ash content and inorganic content of SRF.
2. Based on the SCK method, coal and SRF blends exhibit low to moderate slagging risks with HT and DT levels above 1100 C. However, it should be considered that the risk of corrosion increases due to being at high acid levels.
3. Co-combustion of coal and SRF indicates an increase in Ca-rich particles by 1–3 wt% which can promote the formation of lower melting temperature minerals. Particle size increases as the SRF ratio in the blend increases. In addition, no melting occurred up to 10 wt% SRF in the blend. However, corrosion began to experience at 25 wt% SRF.

Studies on coal-SRF co-combustion, either by using additives, blending with other fuels and different portions, or separating biodegradable- and non-biodegradable-rich waste need to be conducted further.

Acknowledgments

This research was supported financially by the Renewable Energy Program of the Research Organization for Energy and Manufacture, National Research and Innovation Agency. The authors also acknowledge the scientific and technical support provided by the Deputy for Research and Innovation Infrastructure through E-Layanan Sains (ELSA).

Reference

Asim, Mohammad, Mohd T. Paridah, M. Chandrasekar, Rao M. Shahroze, Mohammad Jawaid, Mohammed Nasir, and Ramengmawii Siakeng. 2020. Thermal Stability of Natural Fibers and Their Polymer Composites. *Iranian Polymer Journal* 29 (7):625–648. doi:10.1007/s13726-020-00824-6.

Babu, Renju, Patricia M. Prieto Veramendi, and Eldon R. Rene. 2021. Strategies for Resource Recovery from the Organic Fraction of Municipal Solid Waste. *Case Studies in Chemical and Environmental Engineering* 3 (June). Elsevier Ltd. doi:10.1016/j.cscee.2021.100098.

Chen, Chunxiang, Yingxin Bi, Yuting Huang, and Haozhong Huang. 2021. Review on Slagging Evaluation Methods of Biomass Fuel Combustion. *Journal of Analytical and Applied Pyrolysis*. Elsevier B.V. doi:10.1016/j.jaap.2021.105082.

Conesa, Juan A., and Lorena Rey. 2015. Thermogravimetric and Kinetic Analysis of the Decomposition of Solid Recovered Fuel from Municipal Solid Waste. *Journal of Thermal Analysis and Calorimetry* 120 (2). Kluwer Academic Publishers:1233–1240. doi:10.1007/s10973-015-4396-4.

Das, Samar, Pranay Kumar Sarkar, and Sadhan Mahapatra. 2021. Single Particle Combustion Studies of Coal/Biomass Fuel Mixtures. *Energy* 217 (February). Elsevier Ltd. doi:10.1016/j.energy.2020.119329.

del Zotto, L., A. Tallini, G. di Simone, G. Molinari, and L. Cedola. 2015. Energy Enhancement of Solid Recovered Fuel within Systems of Conventional Thermal Power Generation. In *Energy Procedia*, 81:319–338. Elsevier Ltd. doi:10.1016/j.egypro.2015.12.102.

García, Roberto, Consuelo Pizarro, Ana Álvarez, Antonio G. Lavín, and Julio L. Bueno. 2015. Study of Biomass Combustion Wastes. *Fuel* 148:152–159. doi:10.1016/j.fuel.2015.01.079.

Ghazidin, Hafizh, Hanafi Prida Putra, Nur Cahyo, Ardi Nugroho, Rahmat Ranggonang Anwar, Muhammad Hasan Albana, and Hariana Hariana. 2023. Slagging, Fouling, Abrasion, and Corrosion Potential in Cofiring Biomass SRF With Bituminous Coal Blend. In *Energy Proceedings Volume 31*, 1–6. doi:10.46855/energy-proceedings-10393.

Ghazidin, Hafizh, Suyatno Suyatno, Adi Prismantoko, Feri Karuana, Sarjono, Prabowo, Atok Setiyawan, Arif Darmawan, Muhammad Aziz, Hari Vuthaluru, et al. 2024. Impact of Additives in Mitigating Ash-Related Problems during Co-Combustion of Solid Recovered Fuel and High-Sulfur Coal. *Energy* 292 (April). Elsevier Ltd. doi:10.1016/j.energy.2024.130510.

Ghazidin, Hafizh, Suyatno Suyatno, Adi Prismantoko, Ade Sana Ruhiyat, Prabowo, Arif Darmawan, Mochamad Soleh, Amiral Aziz, Puji Asmanto, Hari Vuthaluru, et al. 2025. Control of Slagging and Fouling during Co-Firing of Solid Recovered Fuel and High-Sodium Coal Using Aluminum and Magnesium-Based Additives. *Energy* 318 (March). Elsevier Ltd. doi:10.1016/j.energy.2025.134873.

Giraud, Robert J., Philip H. Taylor, and Chin-pao Huang. 2021. Combustion Operating Conditions for Municipal Waste-to-Energy Facilities in the U.S. *Waste Management* 132 (August):124–132. doi:10.1016/j.wasman.2021.07.015.

Gunasee, Sanjana D., Marion Carrier, Johann F. Gorgens, and Romeela Mohee. 2016. Pyrolysis and Combustion of Municipal Solid Wastes: Evaluation of Synergistic Effects Using TGA-MS. *Journal of Analytical and Applied Pyrolysis* 121 (September):50–61. doi:10.1016/j.jaap.2016.07.001.

Hariana, Hariana, Adi Prismantoko, Hafizh Ghazidin, Ade Sana Ruhiyat, Nandang Suhendra, Arif Darmawan, Firman Bagja Juangsa, Rachmanoe Indarto, Yibin Wang, and Muhammad Aziz. 2025. Mitigation of Ash Deposition Problem during Co-Combustion of Coal and Refuse-Derived Fuel Using Aluminium-Rich Anti-Slagging Additives. *Journal of the Energy Institute* 120 (June). Elsevier B.V. doi:10.1016/j.joei.2025.102041.

Hariana, Adi Prismantoko, Ganda Arif Ahmadi, and Arif Darmawan. 2021. Ash Evaluation of Indonesian Coal Blending for Pulverized Coal-Fired Boilers. *Journal of Combustion* 2021. doi:10.1155/2021/8478739.

Hariana, Hanafi Prida Putra, Prabowo, Edi Hilmawan, Arif Darmawan, Keiichi Mochida, and Muhammad Aziz. 2023. Theoretical and Experimental Investigation of Ash-Related Problems during Coal Co-Firing with Different Types of Biomass in a Pulverized Coal-Fired Boiler. *Energy* 269 (April). Elsevier BV:126784. doi:10.1016/j.energy.2023.126784.

Huang, Xiankun, Hongchao Yin, Bin Zhang, Ning Mei, and Lin Mu. 2022. Pyrolysis of Lignin (De–Alkaline) via TG/DSC–FTIR and TG–MS: Pyrolysis Characteristics, Thermo-Kinetics, and Gas Products. *Biomass Conversion and Biorefinery*, no. 0123456789. Springer Berlin Heidelberg. doi:10.1007/s13399-022-02387-3.

Isaac, K, and S O Bada. 2022. Co-Firing of High-Ash Discard Coal and Refuse-Derived Fuel-Ash and Gaseous Emissions. *The Journal of the Southern African Institute of Mining and Metallurgy* 122. doi:10.17159/2411.

Kan, Tao, Vladimir Strezov, and Tim J. Evans. 2016. Lignocellulosic Biomass Pyrolysis: A Review of Product Properties and Effects of Pyrolysis Parameters. *Renewable and Sustainable Energy Reviews* 57 (May):1126–1140. doi:10.1016/j.rser.2015.12.185.

Kaniowski, Wiesław, Jan Taler, Xuebin Wang, Izabela Kalemba-Rec, Marcin Gajek, Agata Mlonka-Mędrala, Dorota Nowak-Woźny, and Aneta Magdziarz. 2022. Investigation of Biomass, RDF and Coal Ash-Related Problems: Impact on Metallic Heat Exchanger Surfaces of Boilers. *Fuel* 326 (October). Elsevier Ltd. doi:10.1016/j.fuel.2022.125122.

Karpan, Balasubramanian, Abdul Aziz Abdul Raman, and Mohamed Kheireddine Taieb Aroua. 2021. Waste-to-Energy: Coal-like Refuse Derived Fuel from Hazardous Waste and Biomass Mixture.

Process Safety and Environmental Protection 149 (May). Institution of Chemical Engineers:655–664. doi:10.1016/j.psep.2021.03.009.

Karuana, Feri, Adi Prismantoko, Gaguk Jatisukamto, Barman Tambunan, Nandang Suhendra, Muhammad Syahril, Sri Rahayu, Arif Darmawan, Djarot B. Darmadi, Muhammad Aziz, et al. 2024a. Degradation of the Protective Layer on Stainless Steel by Chlorine Variation under High-Temperature Conditions. *Materials Today Communications* 40 (August). Elsevier Ltd. doi:10.1016/j.mtcomm.2024.109981.

Karuana, Feri, Adi Prismantoko, Arief Wicaksono, Mochammad Noer Ilman, Priyo Tri Iswanto, Arif Darmawan, Muhammad Aziz, Muhammad Akhsin Muflikhun, and Hariana Hariana. 2024b. Effects of Ash Formation during Co-Firing Refuse-Derived Fuel with Coal on Initial Superheater Material Degradation. *Energy Sources, Part A: Recovery, Utilization and Environmental Effects* 46 (1). Taylor and Francis Ltd.:1–15. doi:10.1080/15567036.2024.2390101.

La Mantia, F.P., M. Morreale, L. Botta, M.C. Mistretta, M. Ceraulo, and R. Scaffaro. 2017. Degradation of Polymer Blends: A Brief Review. *Polymer Degradation and Stability* 145 (November):79–92. doi:10.1016/j.polymdegradstab.2017.07.011.

Larionov, Kirill Borisovich, and Alexander Alexandrovich Gromov. 2019. Non-Isothermal Oxidation of Coal with Ce(NO3)3 and Cu(NO3)2 Additives. *International Journal of Coal Science and Technology* 6 (1). Springer Singapore:37–50. doi:10.1007/s40789-018-0229-y.

Li, Jianbo, Mingming Zhu, Zhezi Zhang, Kai Zhang, Guoqing Shen, and Dongke Zhang. 2016. The Mineralogy, Morphology and Sintering Characteristics of Ash Deposits on a Probe at Different Temperatures during Combustion of Blends of Zhundong Lignite and a Bituminous Coal in a Drop Tube Furnace. *Fuel Processing Technology* 149. Elsevier B.V.:176–186. doi:10.1016/j.fuproc.2016.04.021.

Liu, Shunv, Zongde Liu, Yongtian Wang, and Jin Tang. 2014. A Comparative Study on the High Temperature Corrosion of TP347H Stainless Steel, C22 Alloy and Laser-Cladding C22 Coating in Molten Chloride Salts. *Corrosion Science* 83. Elsevier Ltd:396–408. doi:10.1016/j.corsci.2014.03.012.

Liu, Zhuo, Jianbo Li, Mingming Zhu, Quanhai Wang, Xiaofeng Lu, Yuanyuan Zhang, Zhezi Zhang, and Dongke Zhang. 2019. Morphological and Mineralogical Characterization of Ash Deposits during Circulating Fluidized Bed Combustion of Zhundong Lignite. *Energy and Fuels* 33 (3). American Chemical Society:2122–2132. doi:10.1021/acs.energyfuels.8b04512.

Ma, Bao Guo, Xiang Guo Li, Li Xu, Kai Wang, and Xin Gang Wang. 2006. Investigation on Catalyzed Combustion of High Ash Coal by Thermogravimetric Analysis. *Thermochimica Acta* 445 (1):19–22. doi:10.1016/j.tca.2006.03.021.

Maj, Izabella, Sylwester Kalisz, Robert Wejkowski, Marek Pronobis, and Klaudiusz Gołombek. 2022. High-Temperature Corrosion in a Multifuel Circulating Fluidized Bed (CFB) Boiler Co-Firing

Refuse Derived Fuel (RDF) and Hard Coal. *Fuel* 324 (September). Elsevier Ltd. doi:10.1016/j.fuel.2022.124749.

Mlonka-Mędrala, Agata, Tadeusz Dziok, Aneta Magdziarz, and Wojciech Nowak. 2021. Composition and Properties of Fly Ash Collected from a Multifuel Fluidized Bed Boiler Co-Firing Refuse Derived Fuel (RDF) and Hard Coal. *Energy* 234 (November). Elsevier Ltd. doi:10.1016/j.energy.2021.121229.

Mu, Lin, Ranyu Wang, Zhende Zhai, Bin Zhang, Yan Shang, and Hongchao Yin. 2021. Evaluation of Thermokinetics Methodology, Parameters, and Coke Characterization of Co-Pyrolysis of Bituminous Coal with Herbaceous and Agricultural Biomass. *Biomass Conversion and Biorefinery*, April. doi:10.1007/s13399-021-01502-0.

Nasrullah, Muhammad, Pasi Vainikka, Janne Hannula, Markku Hurme, and Janne Kärki. 2015. Mass, Energy and Material Balances of SRF Production Process. Part 3: Solid Recovered Fuel Produced from Municipal Solid Waste. *Waste Management and Research* 33 (2). SAGE Publications Ltd:146–156. doi:10.1177/0734242X14563375.

Novendianto, Ivan Bagus, M. S.K.Tony Suryo Utomo, Muchammad Muchammad, Fairuz Milkiy Kuswa, Hafizh Ghazidin, Feri Karuana, Puji Agus Santoso, Adi Prismantoko, Nur Cahyo, Kusmiyati Kusmiyati, et al. 2024. Investigation of the Slagging and Fouling Aspects of Co-Firing Coal and Organic Refuse-Derived Fuel. *Thermal Science and Engineering Progress* 49 (March). Elsevier Ltd. doi:10.1016/j.tsep.2024.102447.

Pang, Cheng Heng, Sanyasi Gaddipatti, Gregory Tucker, Edward Lester, and Tao Wu. 2014. Relationship between Thermal Behaviour of Lignocellulosic Components and Properties of Biomass. *Bioresource Technology* 172 (November):312–320. doi:10.1016/j.biortech.2014.09.042.

Pettersson, J., J. E. Svensson, and L. G. Johansson. 2008. Alkali Induced Corrosion of 304-Type Austenitic Stainless Steel at 600°C; Comparison between KCl, K2CO3 and K 2so4. In *Materials Science Forum*, 595-598 PART 1:367–375. Trans Tech Publications Ltd. doi:10.4028/www.scientific.net/msf.595-598.367.

Prismantoko, Adi, Feri Karuana, Tito Aziz, FX Guwowijoyo, Sobar Ihsan, and Hariana. 2022. Influence of Coal-Solid Recovered Fuel Blended on Slagging, Fouling and Corrosion During Co-Firing in A Drop Tube Furnace. In *Energy Proceedings Volume 26*, 1–5. doi:10.46855/energy-proceedings-10130.

Prismantoko, Adi, Feri Karuana, Hafizh Ghazidin, Ade Sana Ruhiyat, Nesha Adelia, Moch. Zulfikar Eka Prayoga, Romelan Romelan, Setyo Margo Utomo, Nur Cahyo, Juli Hartono, et al. 2024a. Ash Deposition Behavior during Co-Combustion of Solid Recovered Fuel with Different Coals. *Thermal Science and Engineering Progress* 48 (February):102404. doi:10.1016/j.tsep.2024.102404.

Prismantoko, Adi, Feri Karuana, Ardi Nugroho, Puji Agus Santoso, Hanafi Prida Putra, Arif Darmawan, Muhammad Akhsin Muflikhun, Indro Pranoto, Muhammad Aziz, and Hariana Hariana. 2024b. Effects of Biodegradable- and Non-Biodegradable-Rich Waste Separation on Ash Deposition Behaviour during Coal and Refuse-Derived Fuel Co-Combustion. *Waste Management* 177 (April):158–168. doi:10.1016/j.wasman.2024.01.044.

Qonitan, Fatimah Dinan, I. Wayan Koko Suryawan, and Ari Rahman. 2021. Overview of Municipal Solid Waste Generation and Energy Utilization Potential in Major Cities of Indonesia. In *Journal of Physics: Conference Series*. Vol. 1858. IOP Publishing Ltd. doi:10.1088/1742-6596/1858/1/012064.

Ray, Sudip, and Ralph P. Cooney. 2018. Thermal Degradation of Polymer and Polymer Composites. In *Handbook of Environmental Degradation of Materials*, 185–206. Elsevier. doi:10.1016/B978-0-323-52472-8.00009-5.

Ściubidło, A., I. Majchrzak-Kucęba, and M. Niedzielska. 2019. Comparison of Fly Ash from Co-Combustion of Coal/Solid Recovered Fuel (SRF) and Coal/Refuse Derived Fuel (RDF). In *Journal of Physics: Conference Series*. Vol. 1398. Institute of Physics Publishing. doi:10.1088/1742-6596/1398/1/012015.

Ściubidło, Aleksandra, and Wojciech Nowak. 2018. Co-Combustion of Solid Recovered Fuel (SRF) and Coal and Its Impact on Fly Ash Quality. *Gospodarka Surowcami Mineralnymi / Mineral Resources Management* 34 (2). Polish Academy of Sciences:117–136. doi:10.24425/118651.

Sever Akdağ, A., A. Atimtay, and F. D. Sanin. 2016. Comparison of Fuel Value and Combustion Characteristics of Two Different RDF Samples. *Waste Management* 47. Elsevier Ltd:217–224. doi:10.1016/j.wasman.2015.08.037.

Shin, Jeong Seon, Dowon Shun, Churl Hee Cho, and Dal Hee Bae. 2023. A Study on the Co-Combustion Characteristics of Coal and Bio-SRF in CFBC. *Energies* 16 (4). MDPI. doi:10.3390/en16041981.

Sugiyono, A., I. Febijanto, E. Hilmawan, and Adiarso. 2022. Potential of Biomass and Coal Co-Firing Power Plants in Indonesia: A PESTEL Analysis. *IOP Conference Series: Earth and Environmental Science* 963 (1). doi:10.1088/1755-1315/963/1/012007.

Sun, Guang, Gang Zhang, Jingyong Liu, Deniz Eren Evrendilek, and Musa Buyukada. 2021. Thermal Behaviors, Combustion Mechanisms, Evolved Gasses, and Ash Analysis of Spent Potlining for a Hazardous Waste Management. *Journal of Environmental Sciences* 107 (September):124–137. doi:10.1016/j.jes.2021.02.003.

Suyatno, Suyatno, Hariana Hariana, Adi Prismantoko, Hanafi Prida Putra, Nimas Mayang Sabrina Sunyoto, Arif Darmawan, Hafizh Ghazidin, and Muhammad Aziz. 2023. Assessment of Potential Tropical Woody Biomass for Coal Co-Firing on Slagging and Fouling Aspects. *Thermal Science and Engineering Progress* 44 (September). Elsevier Ltd. doi:10.1016/j.tsep.2023.102046.

Tanaka, Hiroshi. 2016. Thermal Distillation System Utilizing Biomass Energy Burned in Stove by Means of Heat Pipe. *Alexandria Engineering Journal* 55 (3). Faculty of Engineering, Alexandria University:2203–2208. doi:10.1016/j.aej.2016.06.008.

Tang, Zhi, Xiaoping Chen, Daoyin Liu, Yaming Zhuang, Minghua Ye, Hongchan Sheng, and Shaojuan Xu. 2016. Experimental Investigation of Ash Deposits on Convection Heating Surfaces of a Circulating Fluidized Bed Municipal Solid Waste Incinerator. *Journal of Environmental Sciences (China)*. Chinese Academy of Sciences. doi:10.1016/j.jes.2016.02.017.

Tejaswini, M.S.S.R., and Pankaj Pathak. 2023. Co-Combustion of Multilayered Plastic Waste Blend with Biomass: Thermokinetics and Synergistic Effect. *Fuel* 337 (April):127168. doi:10.1016/j.fuel.2022.127168.

Vassilev, Stanislav V., David Baxter, and Christina G. Vassileva. 2013. An Overview of the Behaviour of Biomass during Combustion: Part I. Phase-Mineral Transformations of Organic and Inorganic Matter. *Fuel* 112 (May). Elsevier Ltd:391–449. doi:10.1016/j.fuel.2013.05.043.

Vassilev, Stanislav V., David Baxter, and Christina G. Vassileva. 2014. An Overview of the Behaviour of Biomass during Combustion: Part II. Ash Fusion and Ash Formation Mechanisms of Biomass Types. *Fuel* 117 (PART A). Elsevier Ltd:152–183. doi:10.1016/j.fuel.2013.09.024.

Vekemans, Odile, and Jamal Chaouki. 2016. Municipal Solid Waste Cofiring in Coal Power Plants: Combustion Performance. In *Developments in Combustion Technology*. InTech. doi:10.5772/63940.

Viczek, S. A., A. Aldrian, R. Pomberger, and R. Sarc. 2021. Origins of Major and Minor Ash Constituents of Solid Recovered Fuel for Co-Processing in the Cement Industry. *Waste Management* 126 (May). Elsevier Ltd:423–432. doi:10.1016/j.wasman.2021.03.032.

Viklund, Peter, Anders Hjörnhede, Pamela Henderson, Annika Stålenheim, and Rachel Pettersson. 2013. Corrosion of Superheater Materials in a Waste-to-Energy Plant. In *Fuel Processing Technology*, 105:106–112. doi:10.1016/j.fuproc.2011.06.017.

Wasielewski, Ryszard, Małgorzata Wojtaszek, and Agnieszka Plis. 2020. Investigation of Fly Ash from Co-Combustion of Alternative Fuel (SRF) with Hard Coal in a Stoker Boiler. *Archives of Environmental Protection* 46 (2). Polish Academy of Sciences:58–67. doi:10.24425/aep.2020.133475.

Werther, J, M Saenger, E.-U Hartge, T Ogada, and Z Siagi. 2000. Combustion of Agricultural Residues. *Progress in Energy and Combustion Science* 26 (1):1–27. doi:10.1016/S0360-1285(99)00005-2.

Wojtaszek, Małgorzata, Ryszard Wasielewski, and Stavros Kalaitzidis. 2021. Organic Petrographical Features of Fly Ashes Originating from Coal and Coal-Srf Co-Combustion. *Minerals* 11 (2). MDPI AG:1–10. doi:10.3390/min11020128.

Wu, Hao, Peter Glarborg, Flemming Jappe Frandsen, Kim Dam-Johansen, Peter Arendt Jensen, and Bo Sander. 2011. Co-Combustion of Pulverized Coal and Solid Recovered Fuel in an Entrained Flow

Reactor - General Combustion and Ash Behaviour. *Fuel* 90 (5):1980–1991. doi:10.1016/j.fuel.2011.01.037.

Wu, Lei, Xuguang Jiang, Guojun Lv, Xiaodong Li, and Jianhua Yan. 2020. Interactive Effect of the Sorted Components of Solid Recovered Fuel Manufactured from Municipal Solid Waste by Thermogravimetric and Kinetic Analysis. *Waste Management* 102 (February). Elsevier Ltd:270–280. doi:10.1016/j.wasman.2019.10.054.

Xue, Zeyu, Zhaoping Zhong, Bo Zhang, Jin Zhang, and Xingwang Xie. 2017. Potassium Transfer Characteristics during Co-Combustion of Rice Straw and Coal. *Applied Thermal Engineering* 124. Elsevier Ltd:1418–1424. doi:10.1016/j.applthermaleng.2017.06.116.

Yu, Shijie, Xiaoxiao Yang, Qinghai Li, Yanguo Zhang, and Hui Zhou. 2023. Breaking the Temperature Limit of Hydrothermal Carbonization of Lignocellulosic Biomass by Decoupling Temperature and Pressure. *Green Energy & Environment* 8 (4):1216–1227. doi:10.1016/j.gee.2023.01.001.

Zhang, Jigang, Zijun Liu, Xian Li, Bin Wang, Zhaocai Teng, and Kuihua Han. 2023. Study on Slagging Characteristics of Co-Combustion of Meager Coal and Spent Cathode Carbon Block. *Energies* 16 (2). MDPI. doi:10.3390/en16020736.

Zhang, Shaorui, Xiaoqing Lin, Zhiliang Chen, Xiaodong Li, Xuguang Jiang, and Jianhua Yan. 2018. Influence on Gaseous Pollutants Emissions and Fly Ash Characteristics from Co-Combustion of Municipal Solid Waste and Coal by a Drop Tube Furnace. *Waste Management* 81. Elsevier Ltd:33–40. doi:10.1016/j.wasman.2018.09.048.

Zhou, Song, Cheng Liu, and Lian Zhang. 2020. Critical Review on the Chemical Reaction Pathways Underpinning the Primary Decomposition Behavior of Chlorine-Bearing Compounds under Simulated Municipal Solid Waste Incineration Conditions. *Energy and Fuels* 34 (1):1–15. doi:10.1021/acs.energyfuels.9b02958.

Zhu, Xiaochao, Songjiang Li, Yanshan Wang, Shengquan Zhou, Jian Li, Hong Su, Yunan Sun, Beibei Yan, and Guanyi Chen. 2024. Effect of Torrefaction Atmospheres on the Pyrolysis and Combustion of Torrefied Municipal Solid Waste. *Fuel* 364 (May). Elsevier:131056. doi:10.1016/J.FUEL.2024.131056.

DSPACE

https://dspace.org/

Investigation of ash and combustion characteristics during co-combustion of coal and solid recovered fuel in a laboratory-scale combustor

Prismantoko, Adi; Karuana, Feri; Prayoga, Moch Zulfikar Eka; Darmawan, Arif; Muflikhun, Muhammad Akhsin ...

2026
Taylor & Francis
https://doi.org/10.1080/00102202.2025.2492743
Prismantoko A, Karuana F, Prayoga MZE, et al., (2026) Investigation of ash and combustion characteristics during co-combustion of coal and solid recovered fuel in a laboratory-scale combustor. Combustion Science and Technology, Volume 198, Issue 7, 2026, pp. 1695-1719

Downloaded from a DSpace repository. https://dspace.org/